PREPARATION AND CHARACTERIZATION OF DRUG LOADED CATIONIC ALBUMIN NANOPARTICLES

A Thesis Submitted to
the Graduate School of
İzmir Institute of Technology
in Partial Fulfillment of the Requirements for the Degree of

MASTER OF SCIENCE

in Materials Science and Engineering

by
Sümeyra Çiğdem SÖZER

June 2021
İZMİR

ACKNOWLEDGEMENTS

ABSTRACT

PREPARATION AND CHARACTERIZATION OF DRUG LOADED CATIONIC ALBUMIN NANOPARTICLES

Serum albumin protein behaves as a carrier and transporter for both hydrophilic and hydrophobic drugs. Therefore, albumin could be used in the drug carrier systems. Since albumin nanoparticles have a negative charge under physiological conditions, their anionic drug loading and delivering capacities are restricted. This study aims to obtain higher anionic drug loading capacity by producing cationic bovine serum albumin nanoparticles (cBSA NPs). Firstly, the carboxyl groups of amino acids present on the surface of albumin were conjugated with ethylenediamine to change the charge of albumin from negative to positive. Then, cBSA NPs were obtained using the desolvation process.

Anionic salicylic acid (SA) was used for drug loading studies of the obtained cBSA NPs. SA loading and releasing experiments were studied with UV-Vis and electron paramagnetic resonance (EPR) spectroscopy. In the UV-Vis, the drug loading capacity of cBSA NPs was found to increase ~2 fold, and drug release was slower compared to BSA NPs. For EPR studies, SA was labeled with stable radicals. Spin labels allow the simultaneous monitoring of bound and free drugs in the same sample. The drug was loaded into nanoparticles using two methods. Based on EPR results, it was found that drug was loaded to cBSA NPs with 50% and 93%, and to BSA NPs with 4% and 15% ratios, by desolvation and incubation, respectively. Thus, UV-vis and EPR measurements showed that cBSA NPs have higher SA loading potential and slower release ability compared to anionic albumin nanoparticles.

ÖZET

İLAÇ YÜKLÜ KATYONİK ALBUMİN NANOPARÇACIKLARININ HAZIRLANMASI VE KARAKTERİZASYONU

Serum albümin proteini hem hidrofilik hem de hidrofobik ilaçlar için taşıyıcı bir proteindir. Bu nedenle albümin, ilaç taşıyıcılarının hazırlanmasında sıklıkla kullanılmaktadır. Albümin nanoparçacıkları fizyolojik koşullar altında negatif yüke sahip olduklarından dolayı, anyonik ilaç yükleme kapasiteleri sınırlıdır. Bu nedenle, bu çalışma katyonik sığır serum albümin nanoparçacıkları (cBSA NP) üreterek daha yüksek anyonik ilaç yükleme kapasitesi elde etmeyi amaçlamaktadır. İlk olarak, albüminin yüzeyinde bulunan amino asitlerin karboksil grupları etilendiamin ile konjuge edilerek albüminin negatif yükü pozitife dönüştürülmüştür. Ardından, çözgen uzaklaştırma yöntemi kullanılarak katyonik albümin nanoparçacıkları (cBSA NP) elde edilmiştir.

Elde edilen cBSA NP'ların ilaç yükleme kapasitesini test etmek için anyonik ilaç olan salisilik asit (SA) kullanılmıştır. Salisilik asit yükleme ve salım çalışmaları UV-Vis spektroskopisi ve elektron paramanyetik rezonans (EPR) spektroskopisi kullanılarak analiz edilmiştir. UV-Vis çalışmalarında, cBSA NP'ların ilaç yükleme kapasitesinin ~2 kat arttığı ve ilaç salımının BSA NP'lara kıyasla daha yavaş olduğu bulunmuştur. EPR spektroskopi çalışmalarında, SA ilk önce kararlı radikallerle etiketlenmiştir. Spin etiketler aynı numunedeki bağlı ve serbest ilaçların eş zamanlı izlenmesine olanak sağlamaktadır. İlacın iki farklı yöntem kullanılarak nanoparçacıklara yüklenmesi çalışılmıştır. EPR sonuçlarına göre ilacın, çözgen uzaklaştırma ve inkubasyon yöntemleri ile cBSA NP'larına sırasıyla 50% ve 93%, ve normal BSA NP'larına ise sırasıyla 4% ve 15% oranlarında yüklenebildikleri bulunmuştur. Bu sayede anyonik albümin nanoparçacıkları ile karşılaştırıldığında, cBSA nanoparçacıkları daha yüksek salisilik asit yükleme potansiyeline ve daha yavaş salım kabiliyetine sahip oldukları UV-vis ve EPR teknikleri ile gösterilmiştir.

TABLE OF CONTENTS

LIST OF FIGURES

LIST OF TABLES

CHAPTER 1

INTRODUCTION

1.1. Nanomaterials as Drug Delivery Systems

Drug delivery systems are used to carry therapeutic drugs to a certain region of the body as efficiently as possible. However, the poor solubility of drugs has a restrictive effect on the development of drug delivery systems. Most of the drugs are low water soluble, therefore drugs with poor water solubility usually require the use of high doses in order to increase their therapeutic efficacy in targeted areas (Source: Savjani et al., 2012). However, with recent advancements in drug delivery systems, it attempts to minimize the effect of this drawback. Nanoparticle carriers are the primary focus of these studies at the outset. Drug encapsulation in nanoparticles, such as micelles, liposomes, dendrimers, nanocapsules, nanospheres, and others, increases therapeutic effect and prevents harmful side effects (Source: Li et al., 2019). In the literature, many different types of drug delivery systems have been implemented in the prepared nanoparticle-based therapeutics. Some of these are in clinical use and some are in clinical trials (Table 1.1.) There are good examples of many active liposome-based drug delivery systems that have been licensed by the US Food and Drug Administration (FDA), such as liposomal doxorubicin (Doxil) (Source: Barenholz, 2012) and liposomal amphotericin B (Ambisome) (Source: Kennon et al., 1979).

Table 1.1. Nanoparticle-based therapeutics in clinical use and under clinical investigation. (Source: Sun et al, 2014)

Trade Name	Formulation	Drug	Applications	Phase of Development
Abraxane	albumin-bound NP	paclitaxel	metastatic breast cancer	approved
Ambisome	liposome	amphotericin B	fungal infections	approved
Caelyx	PEGylated liposome	doxorubicin	metastatic breast and ovarian cancer	approved

Table 1.1. (cont.)

DepoCyt	lipodome	cytarabine	lymphoma	approved
Doxil	liposome	doxorubicin	Kaposi sarcoma	approved
Genexol-PM	polymeric micellar NP	paclitaxel	breast cancer	approved
Oncaspar	PEGylated asparaginase	asparaginase	acute lymphoblastic leukemia	approved
NK105	micellar NP	paclitaxel	breast cancer	phase III
BIND-014	polymer matrix	docetaxel	prostate cancer	phase II
CYT-6091	gold NP	tumor necrosis factor α	pancreatic cancer, melanoma	phase I/III
CALAA-01	cyclodextrin-containing polymer	siRNA	solid tumor	phase I

Nanomaterials can be made from biological materials such as proteins, gelatin, and phospholipids for liposomes, as well as chemical materials such as different polymers and solid metal-containing nanoparticles, etc. (Figure 1.1.). Their sizes usually vary from 1 to 100 nm, but some nanoparticles can reach up to 1000 nm in size. Nanoparticles provide numerous advantages in drug delivery systems. Their sizes, shapes, compositions, and surface properties can be easily changed. Apart from other drug carrier systems, nanoparticles provide several additional advantages, including: 1) increases the solubility of poorly soluble drug in water and enables them to be transported to the target at higher doses; 2) provides better protection of drug from the effects of enzymes and the highly acidic environment of some cells; 3) highly targeting drug in a specific area to optimize treatment effectiveness while reducing systemic side effects; 4) regulated drug release over a manageable span of time at specific doses (Source: Sun et al., 2014; Tiwari et al., 2012).
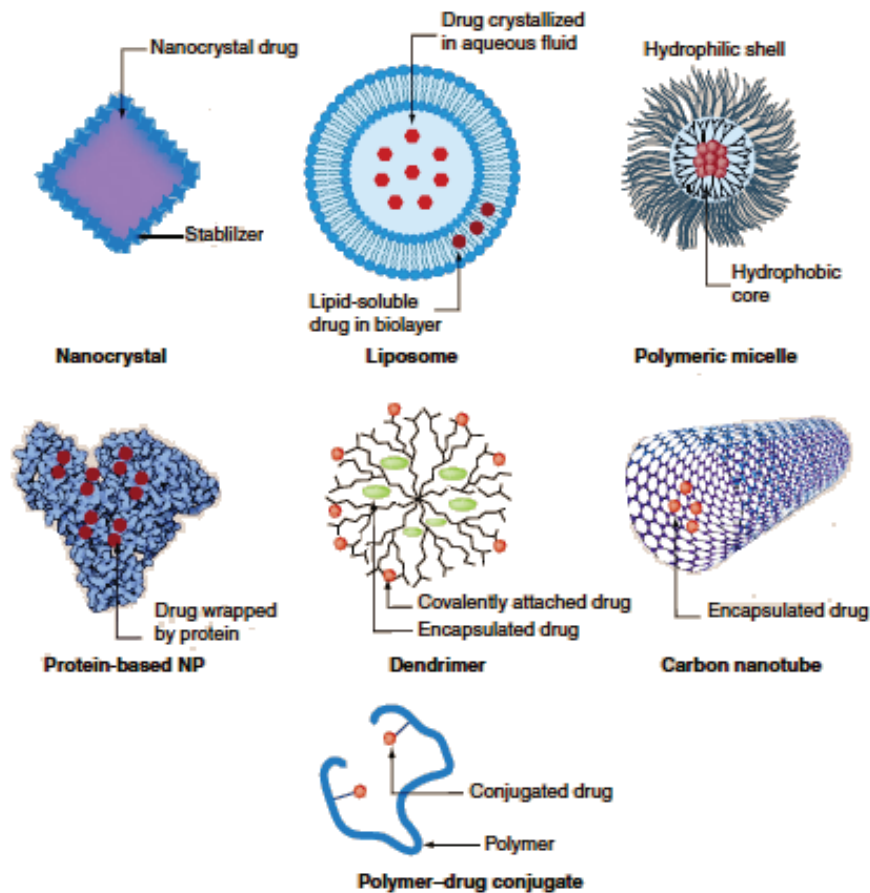
Figure 1.1. Different types of nanomaterials.

(Source: Bamrungsap et al., 2012)

Protein nanocarriers are more favored over the other nanomaterials due to its unique properties like nontoxic, nonantigenic, high binding capacity to drugs, easy to scale up and greater stability (Source: Loureiro et al., 2016). In the literature, different kinds of proteins such as albumin, gelatin, soy, milk, whey, zein and gliadin etc. successfully have been used for the production of protein-based nanoparticles (Source: Lohcharoenkal et al., 2014).

Albumin protein can be derived from a number of sources, including human serum albumin (HSA), bovine serum albumin (BSA), egg white (ovalbumin) or rat serum albumin (RAT). Both HSA and BSA are widely used for the producing albumin nanocarrier systems (Source: Loureiro et al., 2016). Albumin nanoparticles have variety of advantages for the using in drug delivery systems including:

- Biodegradable
- Non-toxic

- Non-immunogenic

- Highly stable during storage

- Easy to scale up and surface charges during producing nanoparticles

- Easy to purify

- Water soluble

- Easy to access

- High capacity for the binding

- Easy to transport drug into body

Since albumin protein has various binding sites (Figure 1.2.), it has a very appreciable impact in loading and transporting of hydrophobic drugs and also positively or negatively charged drugs with electrostatic interactions. The developed albumin nanoparticles with functional groups (carboxyl and amino groups) on its surface can also provide covalently binding to drugs (Source: Hassanin and Elzoghby 2020).
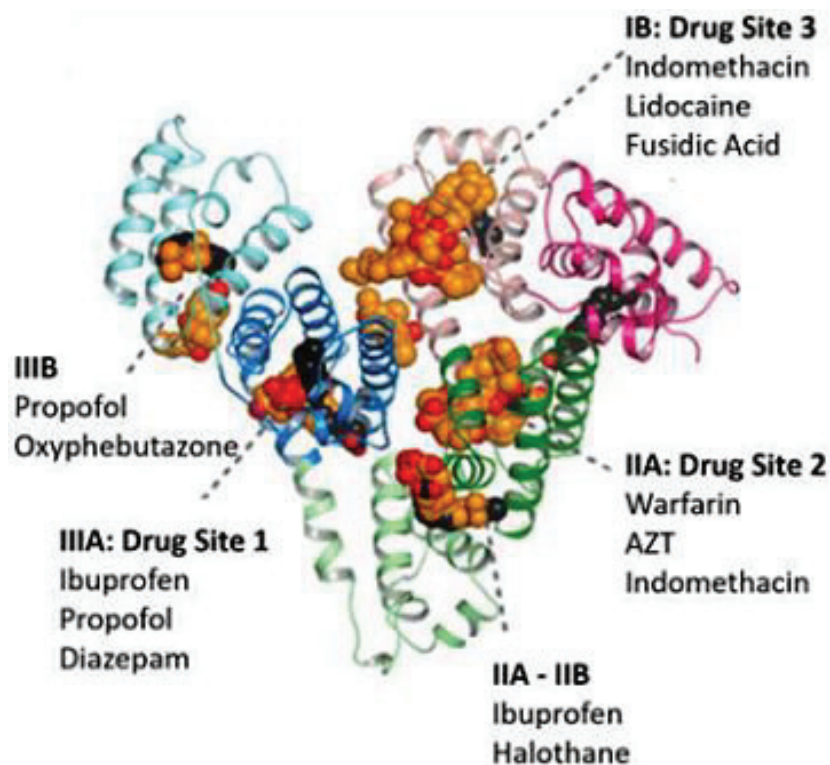
Figure 1.2. Drug binding sites according to the results of HSA-ligand crystal structure studies (Source: Ghuman et al., 2005).

1.2. Bovine Serum Albumin Nanoparticles (BSA NPs) and Drug Interactions

Human serum albumin protein is the most abundant plasma protein in the body (35-50 g/L) which is synthesized in the liver approximately 10-15 g daily. Albumin plays an important role in regulating 80% of the osmotic pressure of the blood, maintaining the pH balance of the plasma and transportation of the nutrients to the cells. Albumin proteins are highly water soluble and remains stable at pH 4-9 over a broad range as well as being thermally stable up to 60 $^\circ$C. Furthermore, albumin increases the solubility and stability of many therapeutic molecules due to its capacity to adhere to hydrophobic and hydrophilic ligand structures, aiding in the improvement of pharmacokinetic properties (Source: Bhushan et al., 2017).

Human serum albumin (HSA) and bovine serum albumin (BSA) are the most commonly used proteins for studies of drug carrier systems. Both HSA and BSA proteins have a molecular weight around 65 kDa and they are homologous proteins with 76% sequence identity (Source: Akdogan et al., 2012). The main distinction between the two that is the number and location of tryptophan residues in each of them. HSA contains only one tryptophan at position 214, which corresponds to Trp-212 for BSA, which is buried in a hydrophobic pocket at subdomain IIA. Also, BSA contains one more tryptophan Trp-134, which is located at subdomain IB. These tryptophan residues provide fluorescence properties to albumin. In most studies, BSA is preferred in drug carrier systems because it is less expensive, biodegradable, and has easier purification properties than HSA (Source: Hassanin and Elzoghby, 2020). Bovine serum albumin has 583 amino acid residues and its isoelectric range between pH 4-9. Its structure in α-helical secondary structure shape and contains 3 main homolog domains (I, II and III) and each domain divided in to two subdomains (A and B) (Figure 1.3). They are connected by 17 disulfide bridges and a free sulfhydryl cysteine-34 (Cys-34) amine residue. Also, albumin contains 2 main binding sites which are site I and site II, they are also known as Sudlow sites. Generally therapeutic molecules bind these Sudlow sites (subdomain IIA or subdomain IIIA) (Source: Kudarha and Sawant 2017; Elzoghby et al, 2012; Fielding et al., 2005).

These Sudlow sites IIA and IIIA are the major binding sites. The site IIA called as 'warfarin binding site' which is large, flexible, multi chamber and located within subdomain IIA. Site IIA is mostly for negatively charged and bulky heterocyclic

compounds such as amantadine and azidothymidin, and they bind to site IIA by hydrophobic interactions. Site IIIA is called as 'indole and benzodiazepine binding site' and it is quite similar to site IIA. However, this site is for more negatively charged compounds like diazepam, ibuprofen, propofol and non-steroid anti-inflammatory drugs. Drugs binds this site by hydrophobic, electrostatic interactions or hydrogen binding. Also, subdomain IB is the secondary binding site for different compounds like indomethacin, naproxen, warfarin, lidocaine, and bilirubin. The structural flexibility of albumin makes albumin nanocarriers a strong carrier mechanism for reversible binding of different molecules to deliver into targeted species (Source: Karimi et al., 2016).
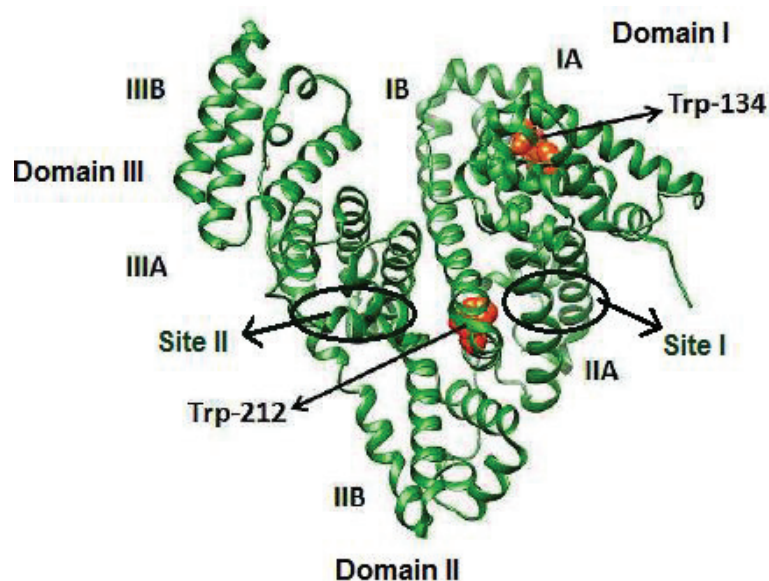
Figure 1.3. Structure of Bovine Serum Albumin (BSA) and its binding sites, domains, subdomains, and tryptophan residues (Source: Prasanth et al., 2016).

Albumin protein can be easily converted into nanoparticles. The use of albumin as nanoparticle ensures that it has many benefits in drug delivery systems, including the ability to disintegrate more quickly, carry more drugs and ligands, and be easily reproduced. Many drugs and ligands can be easily bound to the albumin nanoparticle's surface due to the different reactive functional groups (-SH, -NH$_2$, -COOH) on its surface (Source: Elzoghby et al., 2012). Previous studies in the literature showed that clinical studies can be successfully completed using different methods to incorporate different therapeutic molecules into albumin nanocarrier systems (Table 1.2).

Table 1.2. A summary of clinically approved albumin-related formulations.

(Source: An and Zhang, 2017)

Company	Brand Name	Molecular Type	Status	Clinical Application
GlaxoSmithKline	Albiglutide	Peptide HSA conjugate	Approved	Diabetes mellitus
Abraxis BioScience	Abraxane	Paclitaxel HSA-bound NPs	Approved	Metastatistic breast cancer, lung cancer
Nycomed Amersham	Nanocoll	Tc labelled HSA	Approved	SPECT scan for sentinel node localization in breast cancer
Iso Tex	Jeanatope	Albumin iodinated I-125 serum	Approved	Determination of total blood and plasma volume
Iso Tex	Megatope	Albumin iodinate I-131 serum	Approved	Determination of cardiac output, protein turnover studies
CSL Behring	Alburex	Human Albumin	Approved	Restoration and maintenance of circulating blood volume
Baxter Healthcare Corporation	Aralast NP	Human Albumin	Approved	Emphysema
Merck	Pegintron	Human Albumin	Approved	Cancers of melanoma, leukaemia
Biogen	Avonex	Human Albumin	Approved	Multiple sclerosis
Abbott	Urokinase	Human Albumin	Approved	Blood clots in the lungs

1.3. Albumin Nanoparticle Preparation Techniques

Albumin nanoparticles can be produced using both chemical and physical methods. Emulsification and desolvation methods are at the beginning of chemical methods, and nano spray drying, and thermal gelation methods have recently been used

in physical methods (Source: Elzoghby et al., 2012). The two most widely used techniques are emulsification and desolvation.

In the emulsification method, the aqueous solution of the protein is mixed with a non-aqueous solution (e.g. oil or water immiscible organic solvent) to obtain w/o emulsion. The final nano-sized emulsions are generated using a high-speed homogenizer. To stabilize the formed albumin nanoparticles, a chemical crosslinking agent (e.g. glutaraldeyhde, EDC, formaldehyde) or a thermal crosslinking agent (heated over to 120 ^{0}C) is used as a crosslinker (Figure 1.4) (Source: Khanbabaie and Jahanshahi, 2012; Demirkurt and Akdogan, 2018; Demirkurt et al., 2019) Because of the organic phase used in nanoparticle processing and the surfactants used for stabilization, the emulsification approach necessitates the use of organic solvents to extract the oil residues, which is the key drawback impact. Furthermore, obtaining nanoparticles smaller than 500 nm is difficult (Source: Rahimnejad et al., 2009).
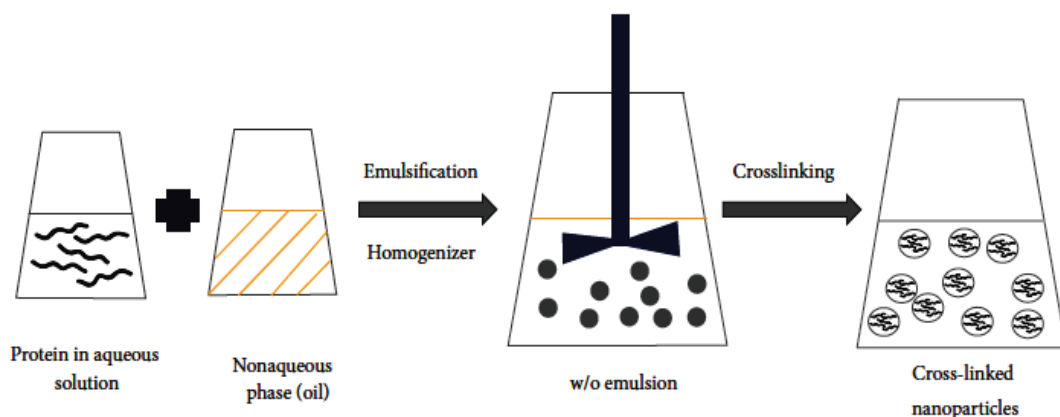
Figure 1.4. Preparation of albumin nanoparticle by emulsification method.
(Source: Lohcharoenkal et al., 2014)

Desolvation method is the most used process for preparation of albumin nanoparticles. In the desolvation process, nanoparticles are produced by continuously adding a desolvating agent such as ethanol or acetone to an aqueous solution of albumin while stirring continuously until the solution becomes turbid. The albumin phase separated after the addition of a desolvating agent to the albumin solution because its water solubility is reduced. Since the morphologically shaped albumin particles were not properly preserved, they could redissolve after dispersion with water. Therefore, coacervates are hardened by crosslinking agent such as glutaraldehyde, in which

albumin's amino moieties in lysine and arginine are connected by the aldehyde-group of glutaraldehyde (Source: Elzoghby et al., 2012). Obtained nanoparticles depend on different factors such as pH of the albumin solution, albumin concentration, stirring rate, desolvating agent and concentration of crosslinker (Source: Loureiro et al., 2016). Figure 1.5 shows the schematically preparation of albumin nanoparticle preparation by the desolvation method.
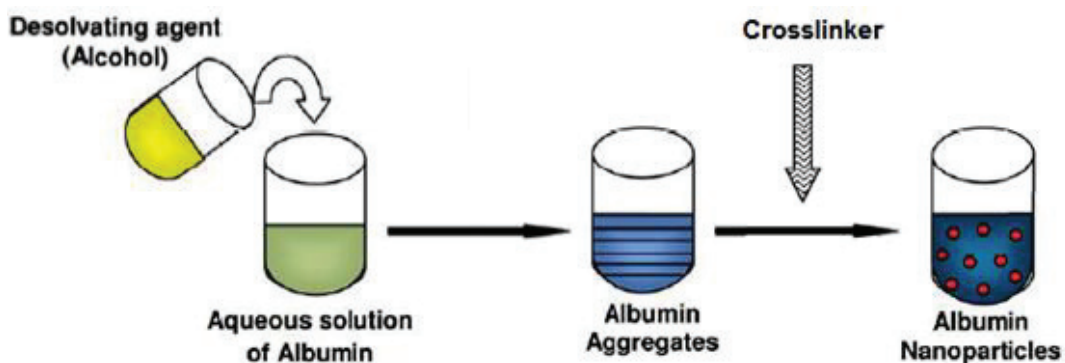
Figure 1.5. Preparation of albumin nanoparticle by desolvation method.
(Source: Khanbabaie and Jahanshahi, 2012)

1.4. Salicylic Acid and Its Interaction with Albumin

Salicylic acid (SA) is component of various plants and its member of salicylates family. Salicylic acid has highly antibacterial, anti-inflammatory, and antifungal properties, therefore it has been used for medications. SA has been identified as a potential treatment for the prevention of cardiovascular disease and cancer by its beneficial properties (Source: Gupta and Dubois, 2001; Paterson and Lawrence, 2001; Amann and Peskar, 2002). SA and salicylates have been used since the fifth century as the active metabolite of aspirin (acetyl SA). However, these salicylic-derived drugs have a 50% bioavailability when administered orally, since they lose their effects after the initial stage of deacetylation to SA. The time of salicylate deacetylation is between 2 and 30 hours (Source: Chandorkar et al., 2014). Also, salicylic acid is an anionic drug and contains two functional groups which are carboxyl (-COOH) and hydroxyl (-OH) groups (Figure 1.6.).
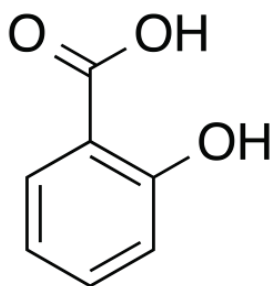
Figure 1.6. Structure of a salicylic acid.

Many studies in the literature have shown that salicylic acid can be loaded or transported by different polymer matrices (Source: Whitaker-Brothers and Uhrich, 2006; Tang et al., 2006; Meng et al., 2014, Nowatzki et al., 2012). Its release can be regulated by the degradation and eventual reabsorption of the sample's polymer matrix by the human body. As a result, gradual and prolonged release of SA could be more effective for the treatment of cancer and cardiovascular disease. Also, the rapid SA release may be needed for antimicrobial and anti-inflammatory purposes, such as infection treatments (Source: Dasgupta et al., 2015).

Ni and his co-workers studied the association between different site markers (warfarin or ibuprofen), salicylic acid, and bovine serum albumin by using spectrofluorimetry (Source: Ni et al., 2006). They used the parallel factor analysis (PARAFAC) algorithm for the analysis of difference between site makers and SA. Based on their results, they concluded that SA has two distinct binding sites in BSA. Site I is a high binding site for warfarin and a low binding site for ibuprofen. Ibuprofen has a high affinity binding site at Site II. Benvidi A., and his team focused on experimental and theoretical approaches for investigate the interactions of bovine serum albumin (BSA) with caffeic acid (CA), salicylic acid (SA), and a combination of these components (Source: Benvidi et al., 2017). They used differential pulse voltammetry (DPV) and UV-vis spectrophotometry (UV-Vis) to analyze interaction between BSA-CA, BSA-SA and mixture of them. They also used chemometric methods including multivariate curve resolution–alternating least squares (MCR–ALS) and parallel factor analysis (PARAFAC) because of the elimination of experimental overlapping signals. According to their DPV and UV-Vis studies, they found SA binds to surface of BSA because the structure and intensities of its DPV and UV-Vis signals are affected by SA binding. As a result, they concluded that hydrophobic interactions are reduced due to electrostatic repulsion between SA and BSA. It was stressed that this may have an effect on the

10

relationship and binding of SA and BSA. In another study, loading of SA to albumin nanoparticles at different pH ranges was studied by using desolvation method (Source: Bronze-Uhle et al., 201). In this study, after salicylic acid was loaded into albumin proteins, it was transformed into nanoparticles with ethanol desolvation. The obtained drug loaded nanoparticles were evaluated with different techniques such as FE-SEM, FTIR and DLS. According to the results of DLS measurements, while the pH value of albumin nanoparticles at pH 7.4, the albumin nanoparticle has low anionic property and although the pH was increased to 9, its anionic properties could not be protected, and it was shown that nanoparticles have gained positive charge with salicylic acid loading. According to the results of the releasing studies of SA, it has been shown that the release of SA occurs immediately in 400 minutes.

It is known that carriers with positively charged groups can enter the cell more easily than neutral or anionic carriers. It has been shown that cationic molecules bind more easily to negatively charged groups such as sialic acid, which initiate uptake on the cell surface (Source: Verma and Stellacci, 2010). In order to increase intracellular uptake of albumin nanocarriers, cationic albumin NPs have been prepared by different methods in the literature. Abbasi and his team prepared Doxorubicin (Dox) loaded cHSA NPs by electrostatically bonding of positively charged polyethyleneimine (PEI) to anionic HSA NPs (Source: Abbasi et al., 2012). In another study, BSA was conjugated with fatty amines in an aqueous environment to form hydrophobic cBSA NPs (Source: Saha et al., 2019). Another research used ethylenediamine conjugation to prepare cBSA proteins, and then electrostatically interacting cBSA with negatively charged siRNAs to produce self-clumping cBSA NPs (Source: Han et al., 2014). Byeon et al. produced Dox-loaded cHSA NPs using an emulsification method and a high-pressure homogenizer after surface-modifying HSA with ethylenediamine (Source: Byeon et al., 2016). It has also been shown that the apparent brain homogenate distribution volume and the post vascular supernatant distribution volume of cationic albumin nanoparticles are ten times greater than that of standard albumin nanoparticles (Source: Triguero et al., 2010).

1.5. Electron Paramagnetic Resonance (EPR) Spectroscopy

Electron paramagnetic resonance spectroscopy (EPR) is a versatile, nondestructive, and powerful technique which is used for the analysis of paramagnetic

species, including organic and inorganic radicals, and paramagnetic triplet states. EPR characterizes the unpaired electrons such as free radicals and transition metals by using microwave radiation (Source: Sahu and Lorigan, 2020). Unpaired electrons move freely in the absence of magnetic field. However, when a magnetic field is applied to electrons, they will adopt different orientations as shown by the quantum number m_s ($m_s = \pm 1/2$). Energies of these two states are proportional to the applied magnetic field B and are given by;

$$E = m_s g \beta B_o \tag{1.1}$$

where B is the Bohr magneton (9.2731×10^{-24} J/T), m_s is the spin quantum number and g is the constant of proportionality factor (2.0023 for a free electron). The energy splitting between the electron spin states called Zeeman splitting. Applying a microwave electromagnetic radiation, electrons can excite from a lower state, $m_s=-1/2$, to a higher state, $m_s=+1/2$ to achieve the resonance condition (Figure 1.7.):

$$h\nu = g\mu_B B \tag{1.2}$$

where h is Planck's constant, ν is the frequency of applied microwave radiation (Hz).
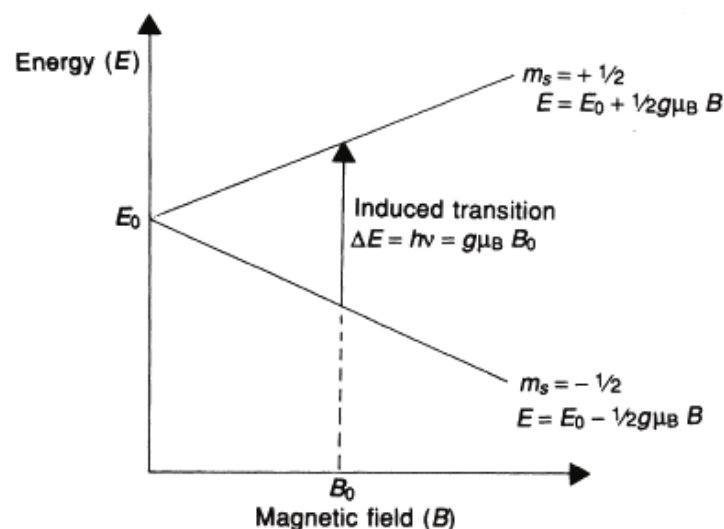
Figure 1.7. Energy level diagram of an unpaired electron in the presence of an external magnetic field, and the EPR transition induced by electromagnetic radiation (Source: Goodman and Hall, 1994).

In EPR experiments, the 9 GHz frequency range is often used, and this range is known as the X-band frequency. Different frequency bands, such as L-band (1 GHz), S-band (4 GHz), K-band (24 GHz), and Q-band (35 GHz), can also be used in the EPR studies. Furthermore, g-value depends on the orientation of the orbital direction of the unpaired electrons effecting from external magnetic field. g_x, g_y and g_z are three characteristic values of g-value and these are along the principal symmetry axes of the orbital.

Generally, EPR spectroscopy collects signals as first derivative of the absorption spectrum. This implies that the peak of absorption refers to the point at which the derivative reaches the baseline. As a result, it is known that first integration of the obtained signal is equal to the standard absorption signal (Figure 1.8.) (Source: Goodman and Hall, 1994).
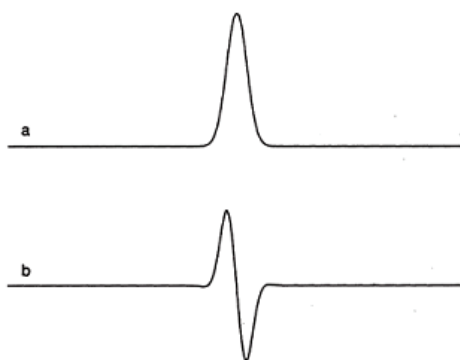
Figure 1.8. EPR line shapes of (a) absorption signal, (b) first derivative of absorption signals.

The magnetic properties of the nucleus that interact with the unpaired electron affect the EPR measurements. The spin magnetic moment of a nucleus with a nuclear spin number (I) is different than zero interacts with the magnetic moment of an electron spin which causes hyperfine coupling. As a result, each of the electron's two energy levels undergoes hyperfine splitting with a number of $2nI +1$, where n is the number of active nucleus. For example, a nitroxyl radical (NO·) have two nuclei, ^{14}N and ^{16}O, with a nuclear spin number 1 and 0, respectively. Therefore, nuclear spin quantum number of ^{14}N, m_I, takes three different values as -1, 0, +1 which results three lines in EPR spectrum (Figure 1.9.) (Source: Spasojević, 2011).
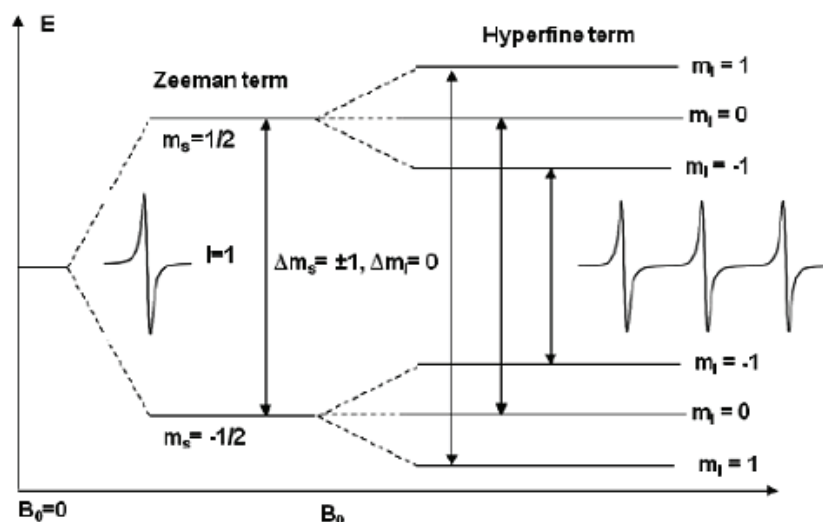
Figure 1.9. Energy level diagram of a nitroxide spin radical in the presence of a magnetic field (B_0), ^{14}N (I=1) hyperfine interaction (Source: Sahu,and Lorigan, 2020).

Spin labeling or spin probing techniques are used in EPR spectroscopy studies to provide analysis of non-paramagnetic materials (Source: Hubbell et al., 2000; Steinhoff 2004; Jeschke and Polyhach, 2007; Akdogan et al., 2012). Spin label molecule binds covalently to non-paramagnetic molecule and makes it EPR active. As a spin label 2,2,6,6-Tetramethylpiperidin-1-oxyl (TEMPO) is widely used by its various forms of tempo-based nitroxide radicals with the difference in its functional groups (-H, -OH, -NH$_2$, -COOH, -N(CH$_3$)$_3^+$). In this study, 4-amino tempo was used as a spin label. (Figure 1.10.) (Source: Tatlidil et al., 2015; Akdogan et al., 2016).
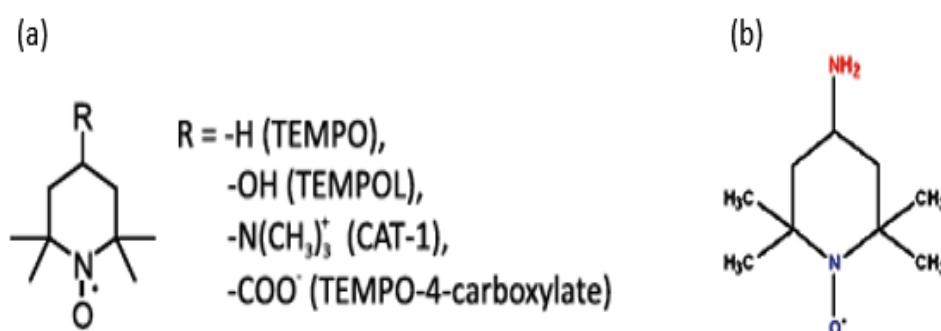
Figure 1.10. Structure of (a) tempo based nitroxide radicals (R: –OH, –NH$_2$, –COOH, –O, –NCS, etc.) and (b) 4-amino-2,2,6,6-tetramethylpiperidine-1-oxyl (4-Amino Tempo). Red-labeled part is the functional group, blue-labeled part is the radical group. (Source: Kattnig et al., 2013).

EPR spectroscopy is widely used to examine the molecular and spherical structure of proteins by applying the spin labeling and spin probing techniques (Source: Hubbell et al., 2000; Steinhoff, 2004; Fajer, 2005; Jeschke and Polyhach, 2007; Akdogan, 2011; Akdogan, 2012). Furthermore, EPR can be used in drug-protein studies (Source: Hauenschild, et al., 2016; Tatlidil et al., 2015; Akdogan et al., 2016). The rotational dynamics of the spin label drugs attached to a large biomacromolecule such as protein gets slower (immobilized) due to the restricted motion of the nitroxyl radicals in the protein bound drug. Consequently, the EPR spectrum consists of broad signals. On the other hand, the EPR spectrum of the free drug (mobilized) with fast rotational speed consists of sharp signals (Figure 1.11.). Therefore, EPR spectroscopy has the ability to observe both the unbound (mobilized) and the bound (immobilized) drug at the same time because of its susceptibility to the rotational dynamics of the radicals. Also, the amount of drugs can be calculated from the areas under the signals (Source: Tatlidil et al., 2015).
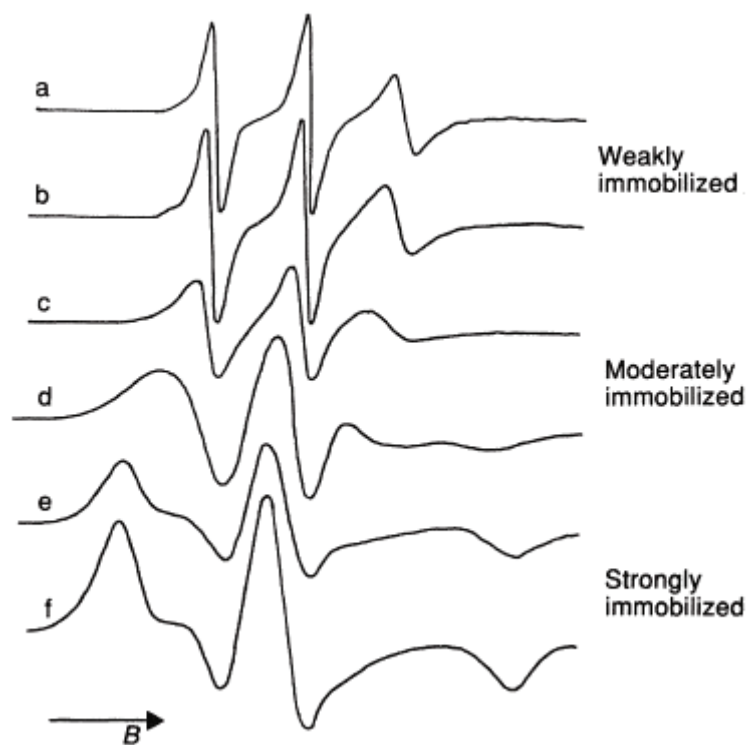
Figure 1.11. Examples of EPR spectral line shapes of a nitroxide spin label.
(Source: Goodman and Hall, 1994)

1.6. Aim of the Study

Albumin nanoparticles are favored in carrier systems because they are non-toxic, biodegradable, and stable over long periods of storage, as well as having a high amine and carboxyl group contents. Also, it is possible to cover them with different ligands or polymers due to the various groups on their surface. The negative charge of the albumin protein under physiological conditions causes the nanoparticles to be negatively charged and therefore the anionic drug loading rates are limited. In the literature, mostly albumin nano-carrier systems have been used to transport drugs with cationic properties. In this study, the carboxyl groups on the surface of the bovine serum albumin (BSA) protein were coated with ethylenediamines to improve anionic drug loadings, and the surface of albumin was converted from negative to positive. In this way, it was aimed to make a more efficient carrier for anionic drugs. Cationic nanoparticle carriers were obtained from the obtained cationic BSA (cBSA) protein by desolvation method. The desolvation method was applied because it provides easier, faster and easier cleaning of the produced nanoparticles than other nanoparticle production methods.

UV-vis absorption, fluorescence, and chromatographic techniques have been used in the literature to determine the binding and releasing ratios of drug loaded albumin nanoparticles (Source: Das et al., 2005; Ni et al., 2006; Lopez et al., 2017). However, it is not possible to study both the bound and unbound drugs simultaneously by using these methods. Electron paramagnetic resonance (EPR) spectroscopy was used as an alternative to the techniques used for drug loading and release measurements. Here, the loading rates and release amounts of the spin-labeled anionic drugs which was chosen as salicylic acid (SLSA), were analyzed by EPR spectroscopy. With EPR spectroscopy, it is possible to determine the released drug and the bound drug simultaneously. In this way, it provides a more reliable detection of loading and released drugs. As a result, in this thesis, drug loading and releasing experiments were evaluated by using EPR spectroscopy in addition to UV-vis and FTIR spectroscopy techniques, which are commonly used in the literature.

CHAPTER 2

EXPERIMENTAL

2.1. Materials

Bovine serum albumin (fatty acid free, lyophilized powder, MW: 66.5 kDa), N-(3-Dimethylaminopropyl)-N′- ethylcarbodiimidehydrochloride (EDC), ethylenediamine (EDA), glutaraldeyhde solution (8% (v/v) in H2O), dimethyl sulfoxide (DMSO), salicylic acid (SA), 4-amino salicylic acid, Tempo-4-amino, dichloromethane, trimethylamine, methanol, and ethyl acetate were purchased from Sigma-Aldrich. Acetonitrile and thiophosgene were purchased from Merck.

Without any further purification, all chemical materials and solvents were used. All the solvents were analytical reagent quality. Distilled water was used to make all the aqueous solutions. Using an OHAUS STARTER3100 pH meter device, the aqueous solutions of EDA and 4-amino salicylic were adjusted using 6M HCl and 12.2M HCl, respectively.

2.2. Preparation of Cationic Bovine Serum Albumin (cBSA)

50 mg of BSA was dissolved in 500 μL distilled water, and then ethylenediamine/water aqueous solution 1.3/1 (v/v) with a pH of 4.75 was added to the BSA solution (9.5 mL). 14.5 mg of EDC was dissolved in 15 mL distilled water and then was added into the mixture of ethylenediamine-BSA in a dropwise manner. The reaction was continued with stirring at 750 rpm for 2 hours. The reaction was terminated by using 1 mL of 4M acetate buffer (pH 4.75). For the elimination of unreacted and excess ethylenediamine and EDC, obtained solution was washed three times with acetate buffer (0.1 M, pH 4.75) and distilled water in an Amicon Ultra (50 kDa MWCO) centrifuge tube at 13,000 rpm for 3 minutes. cBSA was lyophilized and preserved at 4 ^{0}C after being extracted in centrifuge tubes. The yield of the product was 70%.

A Malvern dynamic light scattering (DLS) Nano-ZS instrument (Worcestershire, UK) was used to determine the zeta potentials of cBSA and BSA in aqueous form.

2.3. Preparation of cBSA and BSA NPs

30 mg of lyophilized cBSA (or BSA) was dissolved in 480 µL of water for 20 minutes at 750 rpm stirring. Then, 1920 µL of acetonitrile was added dropwise to the aqueous solution of albumin at a rate of 1 mL / min with a syringe pump and 18 µL of glutaraldehyde solution (8% in H_2O) was added to nanoparticle suspension. After the addition of glutaraldehyde, the reaction was stirred at 750 rpm for overnight. Next, obtained cBSA (or BSA) nanoparticles were transported to eppendorf tubes in order to be centrifuged. Unbound albumins, excess solvents and glutaraldehyde solution were removed by centrifuging the nanoparticles at 14,000 rpm for 45 minutes. The supernatants were removed from the eppendorf and obtained pellets were washed with 3 times by distilled water for the purification of the nanoparticles.

2.4. Characterization of cBSA and BSA NPs

For size and zeta potential measurements, purified NPs were dissolved in distilled water. SEM was used to examine the size and shape of nanoparticles (SEM, FEI QUANTA 250 FEG). Dissolved NPs were diluted 50 times with distilled water. 5 µL solutions of nanoparticles were dropped onto aluminum foil and dried for one day. The dried samples were then coated with gold in a vacuum using an EMITECH K550X for SEM imaging. The accelerating voltages ranged between 5 and 7 kV. In addition, the size of NPs was measured using a Malvern dynamic light scattering (DLS) at a wavelength of 632 nm. The scattering angle was set at 173° and, Malvern dynamic light scattering (DLS) Nano-ZS instrument (Worcestershire, UK) was used to calculate the zeta potentials of nanoparticles.

2.5. Synthesis of Spin Labeled Salicylic Acid (SLSA)

In 32 mL of distilled water, 0.01 mol (1.53 g) of 4-Amino salicylic acid was dissolved and acidified with 3.4 mL of HCl (12.2 M). Following that, 0.044 mol (13.05 g) of thiophosgene was added to the solution of 4-Amino salicylic acid. The mixture was stirred for 1 hour at 0 ^{o}C, then for 2.5 hours at 25 ^{o}C. After filtering the mixture, the

solution was vacuum-dried to produce 4-isothiocyanate salicylic acid. The product was obtained with a 50% yield.

0.625 mmol (107.03 mg) Tempo-4 amino which was used as spin label and 0.46 mmol (89.7 mg) 4-isothiocyanate salicylic acid were mixed and then they were dissolved in 20 mL of DCM. Then a few drops of triethylamine were added to the mixture and

stirred at 25 ^{0}C for overnight. The formed spin-labeled salicylic acid (Spin Labeled Salicylic Acid, SLSA) was purified by column chromatography (ethyl acetate: methanol 15: 1, 13: 1, 12: 1, and 10: 1). The product was obtained with a 46% yield.
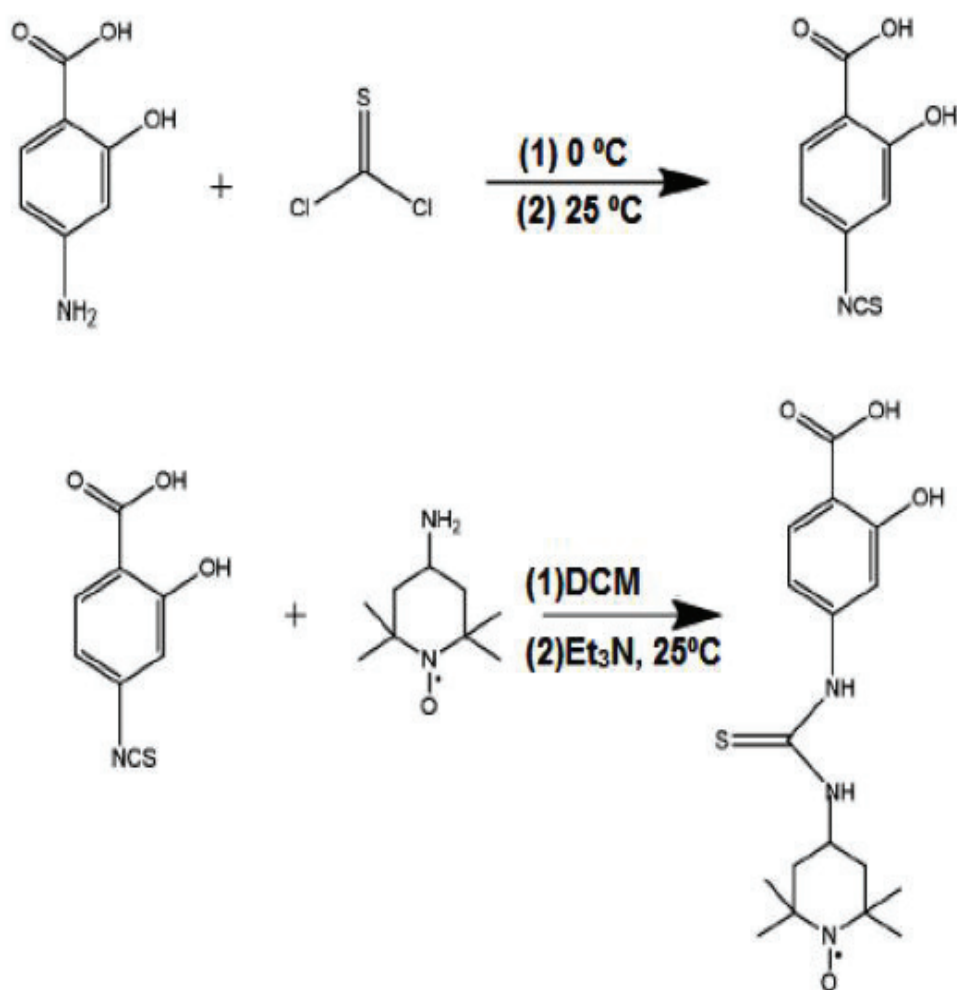
Figure 2.1. Synthesis scheme of spin labeled salicylic acid (SLSA).

2.6. Binding of Salicylic Acid (SA) and Spin Labeled Salicylic Acid (SLSA) to cBSA and BSA NPs

2.6.1. Loading of SA to cBSA and BSA NPs

62.5 mg/mL of lyophilized powder cBSA (or BSA) was dissolved in distilled water for 20 minutes. In DMSO, stock solutions of salicylic acid (SA) were prepared. The albumin solutions were then treated with dissolved SA in the following molar ratios: SA:cBSA (or SA:BSA) 3:1, 5:1, 10:1, 25:1, 35:1, and maintaining the DMSO content stable at less than 2% (v/v). The mixtures were stirred at 750 rpm for 30 minutes. Following the incubation time, acetonitrile was applied dropwise with a syringe pump set to a flow rate of 1 mL/min. The acetonitrile-to-water volume ratio was set at 4:1. Then, 18 µL of 8% (v/v) glutaraldehyde was used as cross-linking agent. A magnetic stirrer set to 750 rpm was used to stir the reaction overnight.

The SA loaded cBSA NPs and BSA NPs were centrifuged at 14,000 rpm for 45 min. Obtained pellets of NPs were lyophilized, and supernatants were collected and analyzed by the UV–visible spectrophotometer to determine the percentage of drug entrapment efficiency (Eq. 2.1) and the percentage of drug loading (Eq. 2.2). Supernatants were diluted with acetonitrile:water (4:1, v/v) to measure the concentration of SA in the supernatants by using LAMBDA 365 UV–visible spectrophotometer (PerkinElmer). For the calibration curve, salicylic acid stock solutions in the acetonitrile:water (4:1, v/v) were prepared. The curve was linear and passed through the origin ($R^2 = 0.9988$, n = 5).

$$Etrapment\ Efficiency\ (\%) = \frac{Initial\ drug\ weight\ -\ Drug\ weight\ in\ supernatant}{Initial\ drug\ weight} \times 100 \qquad (2.1)$$

$$Drug\ Loading\ (\%) = \frac{Weight\ of\ drug\ in\ nanoparticles}{Total\ weight\ of\ nanoparticles} \times 100 \qquad (2.2)$$

2.6.2. Loading of SLSA to cBSA and BSA During NP Formation

30 mg of cBSA protein (or BSA) was dissolved in 480 µL of water and 8.25 µL of SLSA (212 mM) solution prepared in DMSO was added and mixed for 30 minutes. The molar ratio of cBSA: SLSA in the mixture was adjusted to 1: 4. Acetonitrile was used to make nanoparticles and 1920 µL acetonitrile was added dropwise to the albumin-drug solution. Then, glutaraldehyde (18 µL, 8% (v / v)) was added as a crosslinking agent. The mixture was stopped after 4 hours and 7 µL of sample was taken for EPR spectroscopy analysis. Then, 1 mL of the mixture was taken and centrifuged (10 min, 10,000 rpm) and the supernatant was separated. The resulting pellet was dissolved in 1 mL of water. Both samples from supernatant and pellet solutions were measured by EPR spectroscopy. The resulting mole ratio of cBSA NP and SLSA was found to be 1: 7.

2.6.3. Loading of SLSA to cBSA and BSA NPs via Adsorption Method

4 mg of cBSA (or BSA) nanoparticle obtained by desolvation method using acetonitrile was dissolved in 800 µL of distilled water and then mixed with 7.25 µL of SLSA (58.33 mM) prepared in DMSO for 2 hours. 7 µL of experimental medium was taken for EPR measurements. The mixture was then centrifuged (10 min, 10000 rpm) and the supernatant was separated. The resulting pellet was dissolved in 0.8 mL of water. Both samples from supernatant and pellet solutions were measured by EPR spectroscopy. The resulting mole ratio of cBSA NP and SLSA is 1: 7.

All types of drugs loaded nanoparticles were washed 2 cycles with distilled water for the size and zeta potential determinations by using Malvern dynamic light scattering (DLS) Nano-ZS instrument (Worcestershire, UK). Also, their images were obtained by diluting 50 times of the nanoparticles with distilled water for size and shape determinations by using SEM (FEI QUANTA 250 FEG). 5 µL of diluted nanoparticle solutions were dropped to the aluminum foil, and after drying, the samples were coated with the gold by using EMITECH K550X in a vacuum before SEM analyses.

2.7. In Vitro Release Studies of SA/SLSA from cBSA and BSA NPs and Determination by UV-Vis and EPR Spectroscopy

In vitro release of SA from NPs prepared with SA:cBSA and SA:BSA molar ratios 35:1 were perfomed in phosphate buffer (0.1 M, pH 7.4). 6 mg of SA-cBSA NPs and 10 mg of SA-BSA NPs containing the same amount of SA were dispersed in 2 mL of distilled water and 1 mL of phosphate buffer. Then the solutions were transferred in 3 mL D-tube dialyzers (Merck, MWCO 6–8 kDa). The dialyzer tube was placed in a beaker containing 150 mL of phosphate buffer at 37.5 °C under stirring at 200 rpm. At predetermined time points, 2 mL of sample was collected and measured by UV–visible spectrophotometer to determine the released amount of SA from cBSA NPs and BSA NPs. After measurements, the 2 mL of samples were put back in the beakers.

4 mg of SLSA loaded cBSA (and BSA) nanoparticles were dissolved in 0.8 mL of distilled water and inserted in a Pur-A-Lyzer Midi Dialysis tube (MWCO 3.5 kDa). The dialysis tube was then immersed in 32 mL of water and mixed at 650 rpm at 37°C. EPR measurements were obtained at various time intervals from 7 µL of samples collected from the dialysis tube.

2.8. Electron Paramagnetic Resonance Spectroscopy Measurements

For all X-band electron paramagnetic resonance spectroscopy (EPR) analyses, an Adani CMS 8400 benchtop spectrometer with a TE102 resonator cavity was used at a microwave frequency of ~9.4 GHz. Experiments were carried out at 25 °C with a modulation amplitude of 0.1 mT quartz capillary sample tubes were used for the measurements.

2.9. Fourier Transform Infrared Spectroscopy Measurements

Perkin Elmer Fourier Transform Infrared Spectrophotometer (FTIR) equipped with attenuated total reflectance accessory was used for the analyze of synthesized cBSA and drug binding experiments. SLSA loaded cBSA NPs were prepared by using two different drug loading methods, and obtained SLSA, cBSA NPs and SLSA loaded cBSA

NPs were lyophilized for the FTIR measurements. The spectra of the samples were recorded between 4000-600 cm^{-1} wavenumber range with a resolution of 4 cm^{-1}.

CHAPTER 3

RESULTS AND DISCUSSION

The first goal of this study was to produce a good nanocarrier system for the transportation of anionic drugs in the body. For this reason, firstly we synthesized cationic albumin nanoparticles as a model carrier system. Then, the loading of the salicylic acid (SA) which is an anionic drug, to the nanoparticles was characterized by using different spectroscopic methods. UV-Vis spectroscopy was used to determine the loading of salicylic acids into nanoparticles and releasing of salicylic acids from albumin nanoparticles. These studies were only possible with characterization of unbound drugs obtained from the supernatant solutions. Our focus is on EPR spectroscopy since it allows us to analyze both bound and unbound drugs in the same sample. Therefore, we applied spin labeling technique on salicylic acid to analyze binding and release behavior using EPR spectroscopy. FTIR spectroscopy was also used to determine the obtaining cationic BSA (cBSA) and influence of SLSA on the albumin nanocarrier by using different loading methods.

3.1. Characterization of cBSA

In order to synthesize cationic BSA (cBSA), ethylenediamine was used and amide bonds were formed on the protein's surface with amino acids that had carboxyl groups. The ATR-FTIR spectrum shows the cationization of BSA with ethylenediamine (Figure 3.1.). The $C = O$ bond on the side chain carboxylic groups of Asp and Glu in BSA causes the band at 1400 cm^{-1}. As ethylenediamine is conjugated with aspartic acids (Asp) and glutamic acids (Glu), the carboxyl group in cBSA decreases and thus the signal amplitude in this wavenumber decreases.
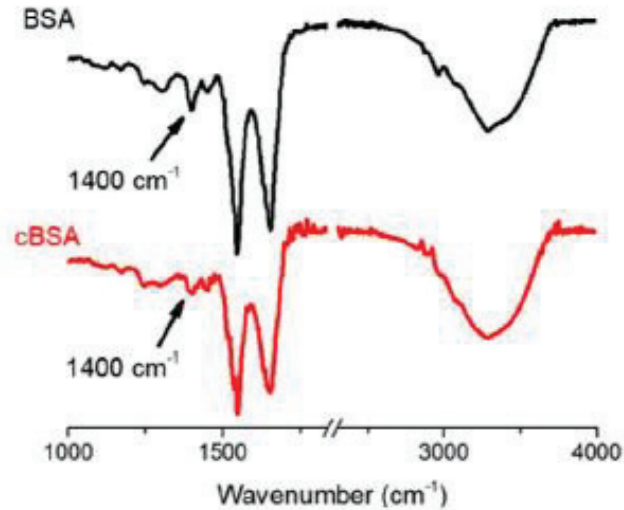
Figure 3.1. ATR-FTIR spectra of native BSA (black) and cBSA aqueous solutions (red). (Source: Sozer et al., 2020)

When BSA was cationized with ethylenediamine, the negative net charge (-11 ± 1) on BSA was converted to a positive net charge (+25 ± 2) at pH 7.0. (Figure 3.2). Furthermore, the zeta potentials of BSA and cBSA at various pH levels (3.0-12.0) were determined. As the pH of BSA was improved from 3.0 to 5.0, the zeta potential decreased from +20 to 0. The zeta potential of BSA decreased as pH increased above the isoelectric point (pI = 5.0). According to the zeta potential findings for cBSA, this indicates that the cBSA has cationic properties by including a large region under the isoelectric point, which was found to be pI = 10.1.
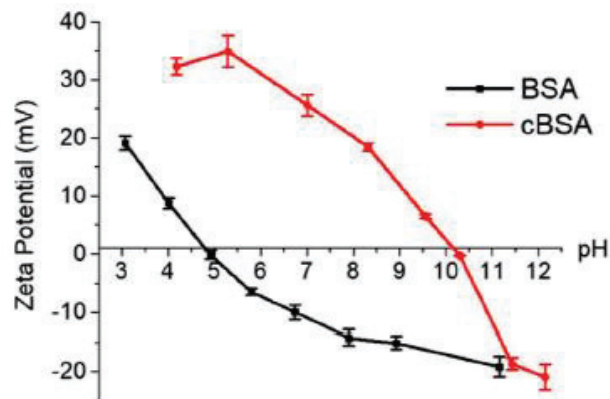
Figure 3.2. The zeta potentials of BSA (black) and cationic BSA (red) proteins at pH values ranging from 3.0 to 12.0 (Source: Sozer et al., 2020).

3.2. Characterization of cBSA and BSA NPs

Desolvation method was used to produce cationic BSA nanoparticles (cBSA NPs) and native BSA nanoparticles (BSA NPs) at pH 7. Acetonitrile was used as the solvent in the desolvation process, and the same solvent was used in all nanoparticle's studies. Considering the previous studies, different solvents were used in the production of albumin nanoparticles and their efficiency under solvent effect was analyzed (Source: Langer et al., 2003; Storp et al., 2012). Acetonitrile was chosen over other solvents such as methanol, ethanol, propanol, isopropanol, and acetone because it has a higher dipole moment ($\mu = 4.00$) (Source: Lee et al., 2003; Rizk and Elenwa, 1968) and, as a polar aprotic solvent, allows for more efficient nanoparticle forming (Source: Sozer et al., 2020). As a result, the extensive electrostatic interaction between acetonitrile and cBSA, as well as hydrophobic interactions and hydrogen bonding, resulted in the producing of more cBSA NPs. The desolation method with acetonitrile produced $54.8 \pm 0.2\%$ cBSA NP and $82.0 \pm 6.5\%$ BSA NP formation.
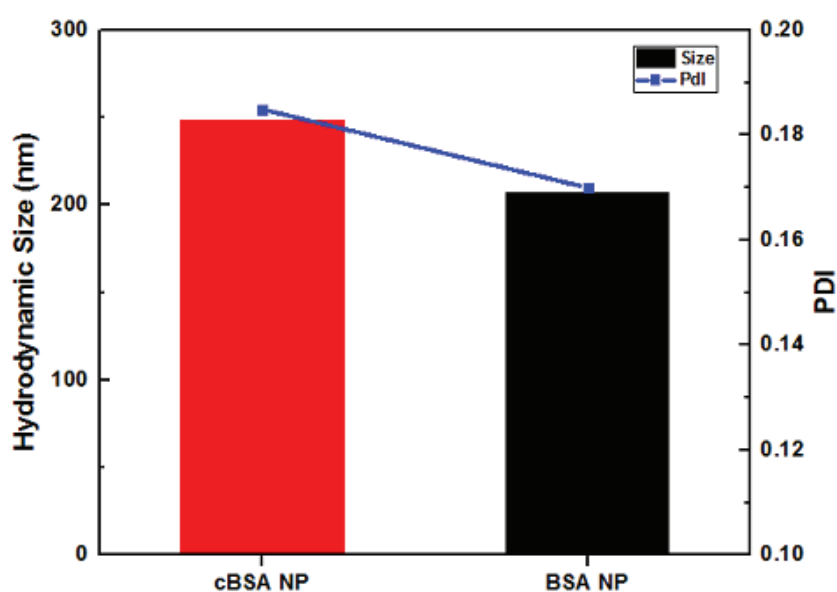
Figure 3.3. The average hydrodynamic sizes and PDI values of cBSA NP (red) and BSA NP (black).

The particle sizes of the obtained nanoparticles were evaluated with a Dynamic Light Scattering (DLS) technique. Figure 3.3. shows the mean hydrodynamic sizes of cBSA NPs and native BSA NPs produced using the desolvation method and their

corresponding polydispersity index (PDI) values. The sizes of obtained cBSA NPs and BSA NPs were found to be approximately 245 ± 4 nm and 202 ± 5 nm, respectively. Also, the corresponding PDI values were found to be 0.18 and 0.16 for cBSA NPs and BSA NPs respectively, PDI values less than 0.2 suggest that these nanoparticles have homogeneous size distribution.

These findings are in good agreement with the nanoparticles' SEM images. Figure 3.4. shows the well dispersed spherical nanoparticles produced by desolvation method. The cBSA and BSA NPs have average sizes range between 100-200 nm.
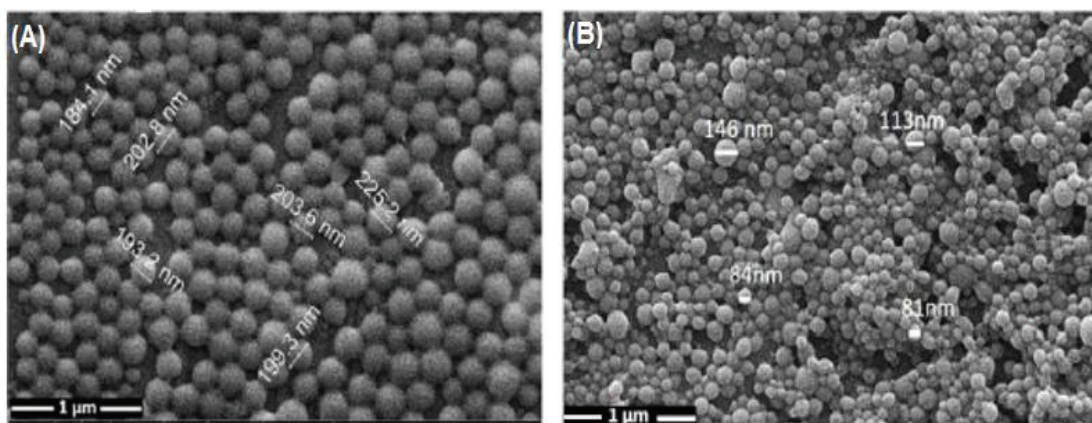
Figure 3.4. SEM images of obtained cBSA NPs (A) and BSA NPs (B).
(Source: Sozer et al., 2020)

The zeta potentials of the produced cBSA NPs were found to be +38 mV. On the other hand, native BSA NPs obtained from non-modified BSA had negative potential charge, -39 mV. These findings indicate that the synthesized nanoparticles have strong stability, with surface charges greater than ±30 mV (Source: Müller et al., 2001).

3.3. Characterization of SA and SLSA Binding to and Release from cBSA and BSA NPs

UV-Vis, EPR and FTIR spectroscopies were used to investigate drug binding to and release from cBSA NPs and BSA NPs.

3.3.1 SA Loading and Release Studies by UV-Visible Spectroscopy

In order to compare of salicylic acid (SA) loading into cationic and anionic albumin nanoparticles, firstly we determined the drug loaded nanoparticles by UV-Vis spectroscopy. Salicylic acid was loaded into nanoparticles by loading SA to the protein during the nanoparticle production process. Salicylic acid is an anionic drug, which is slightly soluble in water, so it was dissolved in DMSO and prepared as a stock in various concentrations. SA from different concentrations bound to proteins by applying it to the aqueous protein solution, and the desolvation process was completed by the additions of acetonitrile and glutaraldehyde for drug loaded nanoparticle formation.

Lyophilized SA loaded NPs and their supernatants were used for calculations of the percentage of entrapment efficiencies (Eq. 2.1) and the percentage of drug loading (Eq. 2.2). Supernatants were diluted with acetonitrile:water (4:1 (v/v)) to calculate concentration of SA in supernatants.
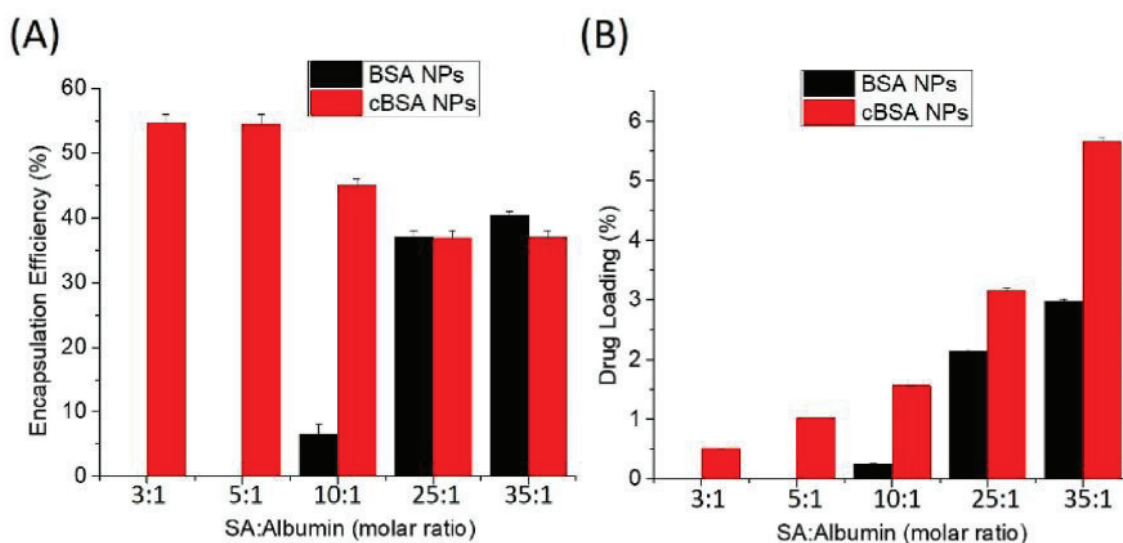
Figure 3.5. (A) Salicylic acid (SA) encapsulation efficiency (wt%) results and (B) SA loading (wt%) results of cBSA NPs (red) and BSA NPs (black) with respect to the initial molar ratio of SA:Albumin (Source: Sozer et al., 2020).

Figure 3.5 (A) shows the SA encapsulation efficiencies (wt%) of cBSA NPs and BSA NPs. The SA entrapment efficiency of nanoparticle was found to be 55 wt% by addition of SA to the cBSA protein (SA:cBSA) at low molar ratios of 3:1 and 5:1. When SA molar ratios were increased to 10:1, 25:1 and 35:1, the nanoparticle entrapment

efficiencies were changed to 45, 37 and 37 wt%, respectively. In addition, the loading amounts of SA added to cBSA NPs were shown in figure 3.5 (B). It was observed that as the molar ratio of SA increased, the drug loading amount in the NP increased. When the SA molar ratio was 35:1, the weight ratio of SA in NP reached to 5.6 wt%. SA loading ratios have been studied up to 35:1 because then the SA solubility decreases in the aqueous medium.
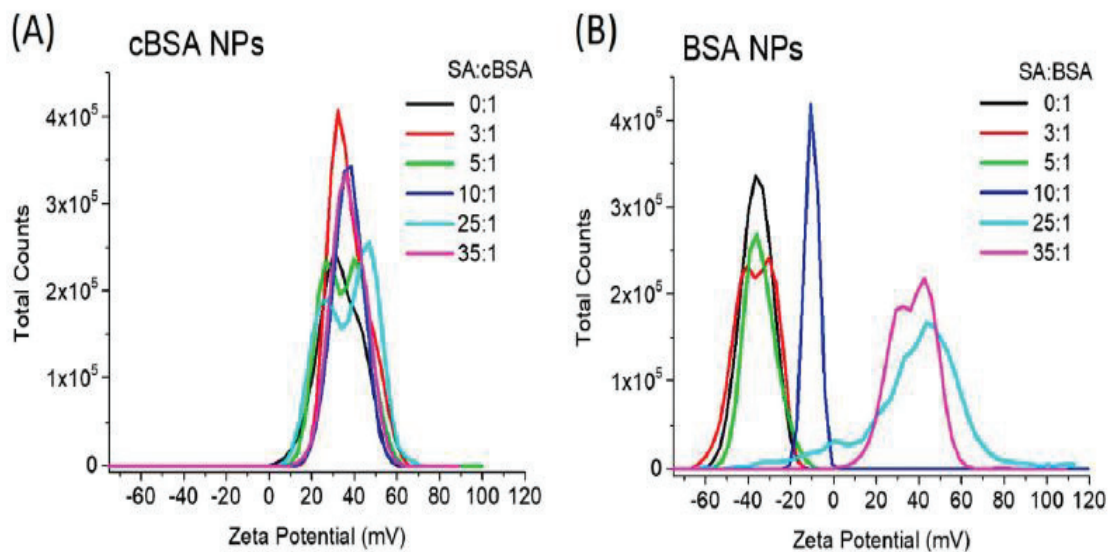
Figure 3.6. The zeta potentials of (A) SA loaded cBSA NPs and (B) SA loaded BSA NPs produced with different SA:cBSA and SA:BSA molar ratios, respectively (Source: Sozer et al., 2020).

In contrast, SA loading to the native BSA NP is not possible at lower molar ratios such as 3:1 and 5:1 (SA:BSA) (Figure 3.5 (A)). Nevertheless, as the SA molar ratio increased to 10:1, 25:1, and 35:1, the encapsulation efficiency on the BSA NPs were found to be 6, 37, and 40 wt%, respectively. Furthermore, when the SA:BSA molar ratios were set to 10:1, 25:1, and 35:1, the SA loading results were found as 0.2, 2.1, and 3.0 wt%, respectively (Figure 3.5 (B)). These findings indicate that SA loading to native BSA NP is only possible at higher SA molar ratios. This can be explained through BSA cationization as a result of the larger amount of SA addition in the medium. It was determined that the addition of SA in BSA aqueous solution ratios as 10:1, 25:1 and 35:1 lowered the pH of the albumin solution to 6.1, 5.0 and 4.6, respectively. In these pH ranges, albumin falls below its isoelectric point and its surface charges started to cationization without conjugation of ethylenediamine. With the SA molar ratio reaching

to the 10:1, it was started to load on BSA and, the surface zeta potential of BSA NP was reached from -36 mV to -10 mV, as seen in figure 3.6 (B). At the higher molar ratios of SA such as 25:1 and 35:1, BSA NPs were increased the surface charges even more, reaching to +37.5 and +36.9 mV. As a result, similar to the +40 mV zeta potentials of SA loaded cBSA NPs (Figure 3.6 (A)), unmodified BSA NPs show positive net charges in the presence of high SA levels.
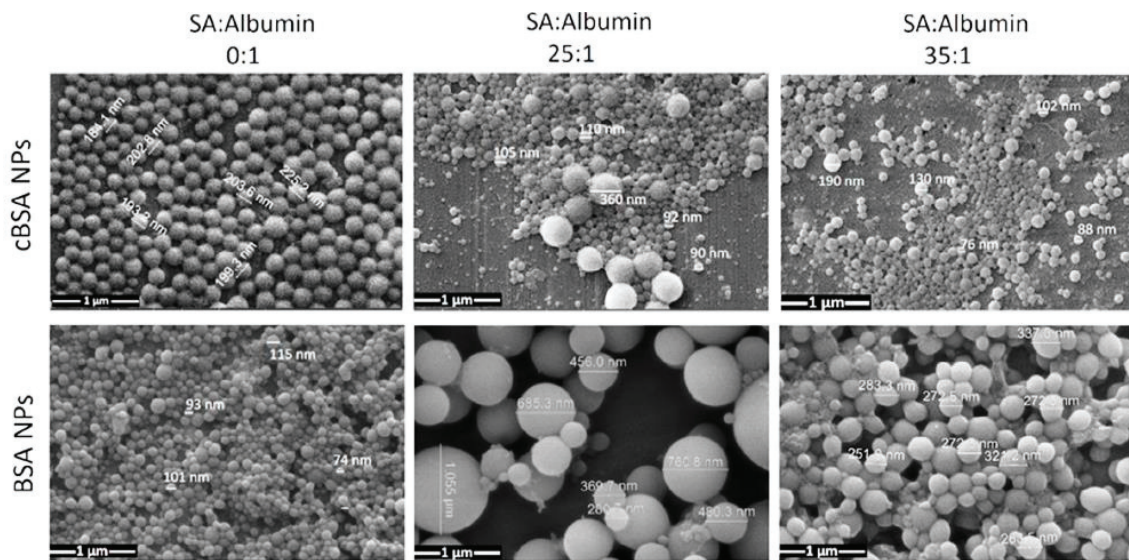
Figure 3.7. SEM images of cBSA NPs (top, left) and BSA NPs (bottom, left) without SA loading. Drug loaded cBSA NPs (top) and BSA NPs (bottom) obtained with mixtures of 25:1 (middle) and 35:1 (right) SA:Albumin molar ratios (Source: Sozer et al., 2020).

In addition, the changes in the size of the cBSA and native BSA NPs with the loading of salicylic acid were analyzed by SEM. Figure 3.7 shows SEM images of cBSA and BSA NPs loaded with SA at different molar ratios such as 0:1, 25:1, and 35:1. Loading SA into cBSA NPs resulted in a gradual decrease in nanoparticle size. The cBSA nanoparticles were in the size range of about 200 nm before SA loaded, but their average size was decreased to around 100 nm with the loading of SA. With the addition of SA at higher molar ratios (25:1 and 35:1 SA:cBSA), the pH value of the cBSA aqueous solution was reduced to 5 therefore cBSA proteins were became more cationic. As a result, higher electrostatic repulsive forces reduced the number of cBSA proteins involved in the aggregation process, resulting in smaller particle formation. The hydrodynamic size results of the obtained nanoparticles with DLS agree with SEM results. The average

hydrodynamic sizes of cBSA NPs decreased from 244 nm (PDI: 0.2) to 182 nm (PDI: 0.22) and 170 nm (PDI: 0.21) upon the SA loadings with 25:1 and 35:1 SA:cBSA molar ratios, respectively.

Contrarily, it was noticed that when SA was loaded into native BSA NPs, the size of the nanoparticles increased significantly from ~100 nm to ~650 nm in a 25:1 molar ratio (Figure 3.7 (bottom)). When the 35:1 molar ratio was used, the nanoparticle size was reduced to ~250 nm. SA effects on the surface charge of the BSA protein in solution. The addition of SA to BSA solution at 25:1 and 35:1 molar ratios (SA: BSA) reduced the pH from 7.0 to 5.0 and 4.6, respectively. The albumin isoelectric point was analyzed to be 5.0 (Figure 3.2.), implying that the albumin isoelectric point is reached at a molar ratio of 25:1. It induces more protein-protein hydrophobic interactions between BSA proteins in the isoelectric range, resulting in larger protein nanoparticles formation. As SA is used in a 35:1 molar ratio, the pH of albumin falls below the isoelectric point and they become cationic, which partly prevents the formation of larger nanoparticles, but they are nevertheless larger NPs as compared to native BSA NPs.

Their SEM results supported their average hydrodynamic sizes. The average sizes of BSA NPs (193 nm, PDI: 0.17) increased to 735 nm (PDI: 0.284) and 268 nm (PDI:0.10) at 25:1 and 35:1 M ratios (SA:BSA), respectively.
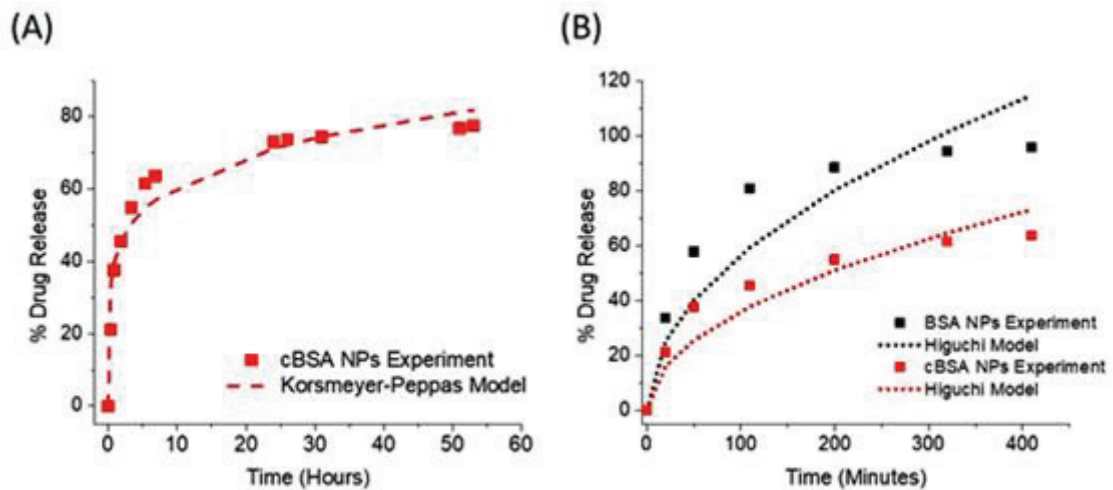
Figure 3.8. The cumulative percentages of SA released from the cBSA NPs within 53 hours with Korsmeyer-Peppas fitting model. (B) The cumulative percentages of SA released from the cBSA NPs (red) and BSA NPs (black) prepared with the 35:1 (SA:Albumin) molar ratio.
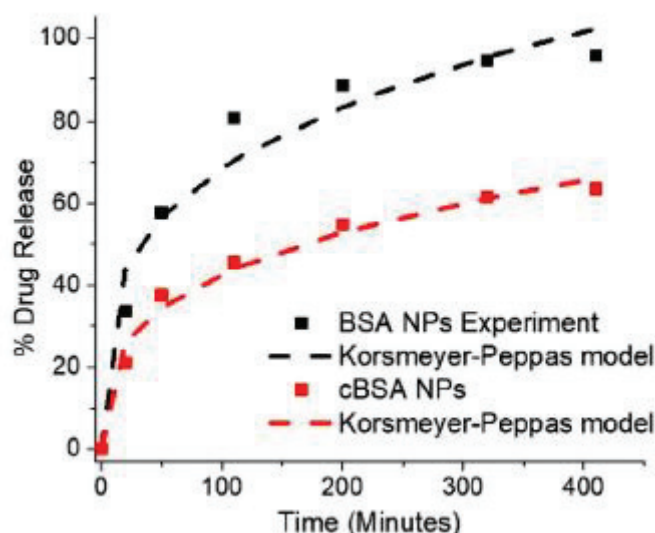
Figure 3.9. The cumulative percentages of SA released from the cBSA NPs (red) and BSA (black) (Source: Sozer et al., 2020).

Also, we performed the release studies of SA from cBSA NPs and BSA NPs. The drug loaded NP ratio was set at 35:1 mol ratio and it was investigated at 37 ^{0}C in 0.1 M phosphate buffer, pH 7.4 (Figure 3.8). The releasing percentage of salicylic acid from the cBSA nanoparticle 78% at the end of 58 hours (Figure 3.8 (A)). In the first 50 minutes, 37% of SA was realized with a sudden burst. Therefore, the release of SA was slow during the ongoing period. SA was released rapidly from the native BSA NPs, with 58% in 50 minutes (Figure 3.8 (B)). The total SA release from BSA NPs was found to be around 100% at the end of 7 hours.

Additionally, SA release results from cBSA NPs and BSA NPs were evaluated mathematically by Higuchi model and Korsmeyer-Peppas model (Source: Karami et al., 2020). Fitting models of SA were shown in figure 3.8 (B) and figure. 3.9. For both BSA NPs and cBSA NPs, the SA release method adopted the Korsmeyer-Peppas model, with higher correlation (R^2) values of 0.98 and 0.99, respectively (Figure 3.9). Also, Higuchi models show R^2 values of 0.94 and 0.97 for BSA NPs and cBSA NPs, respectively (Figure 3.8 (B)). The Korsmeyer-Peppas model's release power (n) value also shows the mechanism of drug release from the carrier. Values of n less than 0.43 for spherical carriers mean that the drug release system relies on the Fickian diffusion mechanism (Source: Ritger and Peppas, 1987). The n values obtained using Korsmeyer-Peppas models are 0.28 and 0.30 for BSA NPs and cBSA NPs, respectively, and it shows that Fickian diffusion controls the release of SA from both NPs. Furthermore, the SA release

rate constants (k) obtained from the Korsmeyer-Peppas model are 19 and 10, respectively, for BSA NPs and cBSA NPs. Therefore, it shows the drug release rate of non-modified BSA NPs is significantly higher than that of cBSA NPs.

BSA NP had a positive charge with the loading of SA, which was changed its the surface charges again to -39 mV with the release of salicylic acids. However, there was no difference in surface charge after the salicylic acid was released from the cBSA NPs. As a result, long-term electrostatic activity between cBSA and SA slows the drug release.

3.3.2 SLSA Loading and Release Studies by EPR Spectroscopy

In order to analyze the loading of salicylic acids into albumin nanocarriers by EPR spectroscopy in detail, first SA was labeled with a spin label. The spin label has been added to the benzene ring to avoid interfering with the functional groups of salicylic acid. For this reason, 4-amino salicylic acid was used as the starting source, and it was converted into 4-isothiocyanate salicylic acid. Spin labeled salicylic acid was obtained from the reaction of isothiocyanate with the amine group of Tempo-4-amino which was used as the spin label (spin labeled salicylic acid, SLSA) (Figure 2.1). Thus, the carboxyl and hydroxyl groups of salicylic acid were not affected by the spin label. EPR measurements of the salicylic acid molecule labeled with Tempo-4-amino showed that the Tempo radical was bound to the salicylic acid molecule. Figure 3.10 shows the EPR spectra of the salicylic acid molecule labeled with Tempo-4-amino and the free Tempo-4-amino radical. The decrease in the signal in the high magnetic field indicates that the Tempo radical was bound to the salicylic acid molecule. The decrease of the signal was due to the slowing or restriction of the rotational movement of the tempo radical after binding to the salicylic acid molecule.
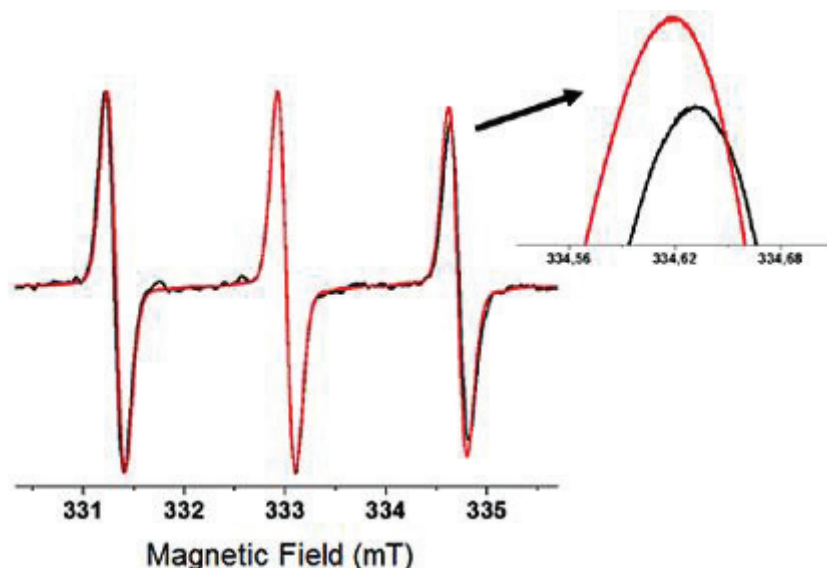
Figure 3.10. EPR spectra of a salicylic acid molecule labeled with Tempo-4-amino (black) and a free Tempo-4-amino radical (red). The thumbnail shows a comparison of the signals shown in the strong magnetic field to help see the contrast between the two spectrums.

In order to characterize SLSA loading into the cationic albumin nanoparticles by EPR spectroscopy two different methods were applied. In the first method, the drug was loaded during nanoparticle production. In the second method, the drug was loaded after the nanoparticle was obtained (incubation method). EPR spectroscopy was used to compare drug loading levels in these different systems. Also, the cBSA:SLSA mole ratio is 1:7 in both methods.

Figure 3.11 shows simultaneously how much of the SLSA drug loaded during the desolvation method. After centrifuging the solution of desolvation experiment, drugs found in pellet and supernatant were measured separately, too. As a result of the double integration of the EPR spectra, the area under the signal was found and the amount of free and bound drug can be compared (Figure 3.11 (B)). Approximately 50% of the added drug remained in the nanoparticle. In the repetition of the same experiments with anionic BSA nanoparticles, it was found that the drug was not bound to nanoparticles significantly. The fact that the pellet signal seen in Figure 3.12 which is very low (4%) and the immediate release of the bound drug in water shows that there is no strong binding.

34
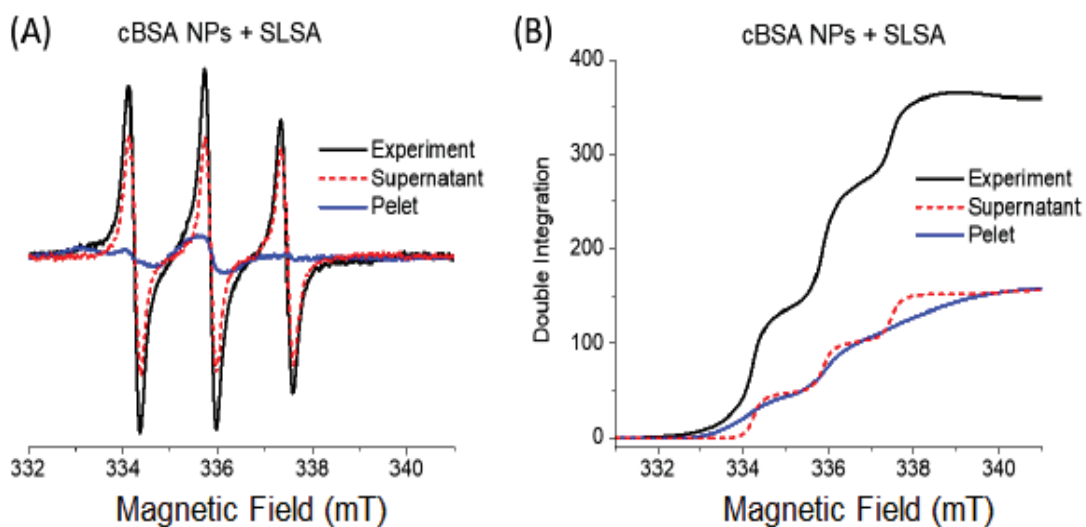
Figure 3.11. (A) EPR spectra of the desolvation experiment mixture, pellet and supernatant obtained by adding the SLSA to the cBSA solution during the desolvation method. (B) Representation of the signal area as a result of the double integrals of the EPR spectra.

Figure 3.12. (A) EPR spectra of the desolvation experiment mixture, pellet and supernatant obtained by adding the SLSA to the BSA nanoparticles obtained after the desolvation method. (B) Representation of the signal area as a result of the double integrals of the EPR spectra.

In another method applied to increase the loading of drugs to nanoparticles, SLSA solution was incubated with nanoparticles. Albumin protein:SLSA mole ratio was again kept at a ratio of 1:7. Figure 3.13 shows how much of the drug was free and how much of drug was bound to the nanoparticle after the incubation method. As a result of the double integration of the EPR spectra, the area under the signal is found and the amount of free and bound drug can be compared (Figure 3.13 (B)). Approximately 93% of the added drug was encapsulated in the cBSA nanoparticle. In repeating the same experiments with anionic BSA nanoparticles, it has been shown that 15% of the added drug can be encapsulated by nanoparticles (Figure 3.14). However, the loaded drug was released immediately in the solution.
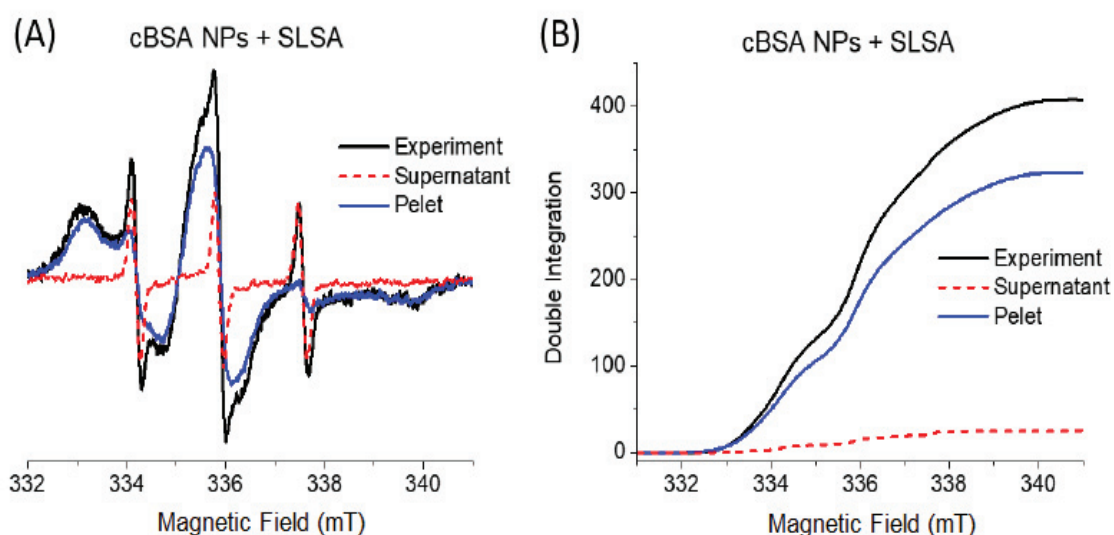
Figure 3.13. (A) EPR spectra of the incubation mixture, pellet and supernatant obtained by adding the SLSA to the cBSA nanoparticle solution by the incubation method. (B) Representation of the signal area as a result of the double integrals of the obtained EPR spectra.
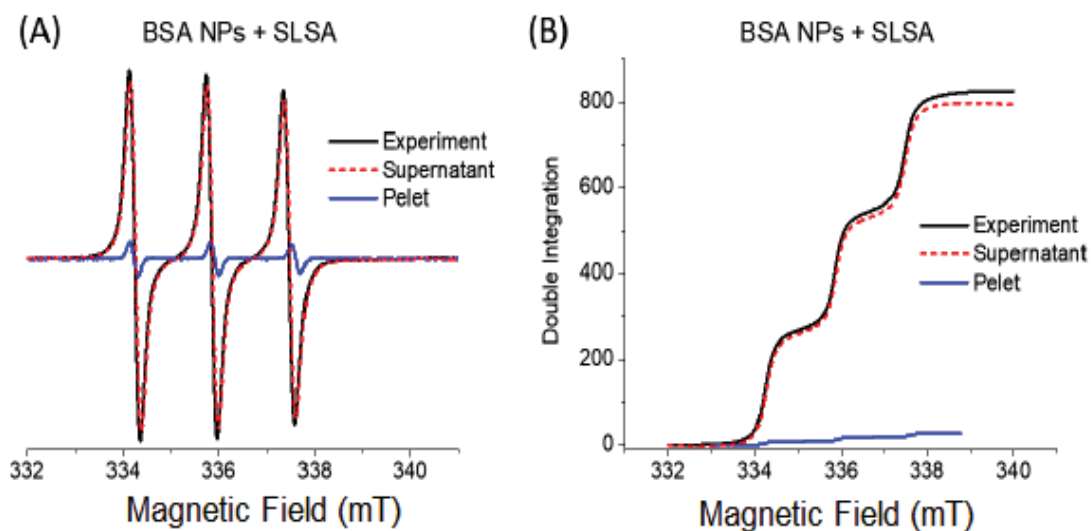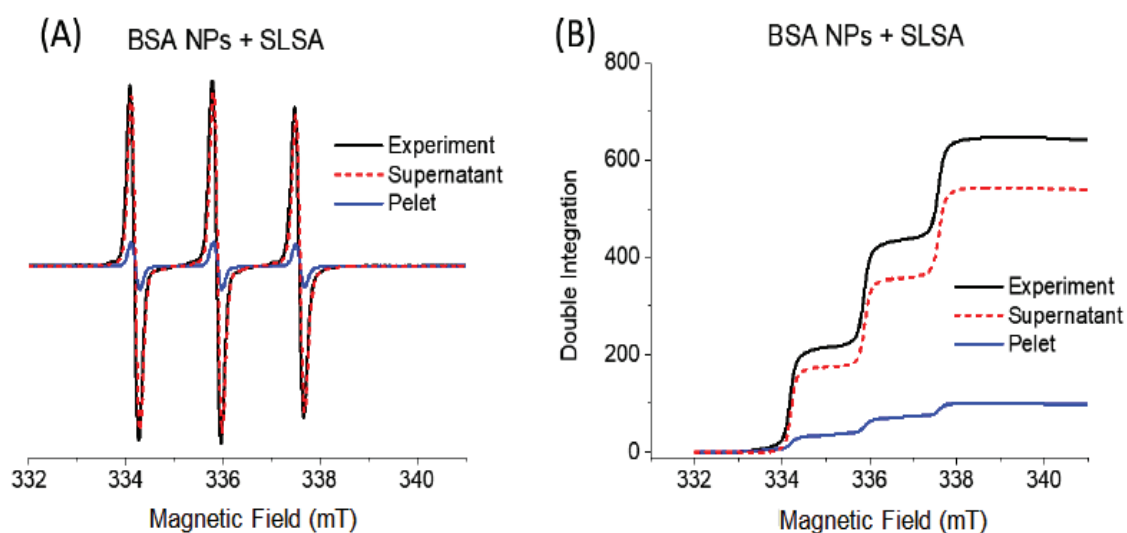
Figure 3.14. (A) EPR spectra of the incubation mixture, pellet and supernatant obtained by adding the SLSA to the BSA nanoparticle solution by the incubation method. (B) Representation of the signal area as a result of the double integrals of the obtained EPR spectra.

Table 3.1. SLSA loading results on cBSA and BSA NPs.

Types of Nanocarrier	Drug Loading Method	Bound Drug (%)	Unbound (Free) Drug (%)
cBSA NP	Desolvation	50	50
BSA NP	Desolvation	4	96
cBSA NP	Incubation	93	7
BSA NP	Incubation	15	85

Table 3.1 shows the results of loading SLSA to both anionic and cationic albumin nanocarriers with using two different loading methods as evaluated by EPR spectroscopy. In the desolvation method, the SLSA can be loaded into cBSA NPs by 50% ratio, while almost no SLSA can be loaded into anionic BSA NPs. It has been found that up to 15% of SLSA can be loaded into the anionic BSA NPs by the incubation method, but this rate is quite high with 93% in cBSA NPs. As summarized in the table, it is more successful to load the anionic drugs into the cationic albumin nanoparticles.

Also, EPR spectroscopy was used to determine the amount of drug released from drug-loaded cBSA nanoparticles obtained from two drug loading methods. Figure 3.15 shows the release dynamics of the drugs loaded during the incubation and desolvation

methods at 37 ^{0}C in water. The amount of drug remaining in the nanoparticle was found from the EPR measurements of the samples taken from the dialysis tube with time. The decrease in the EPR signal gives the amount of drug released. A rapid drug release was observed within the first 5 hours of the drug loaded with incubation. It was found that the loaded drug was released by about 35%. Over time, drug release was very slow and, after 30 hours, a total of 46% of the drug was released. On the other hand, the drug loaded during the nanoparticle synthesis (via desolvation method) was not released. It was observed that the drug remained in the nanoparticle at the end of 48 hours.
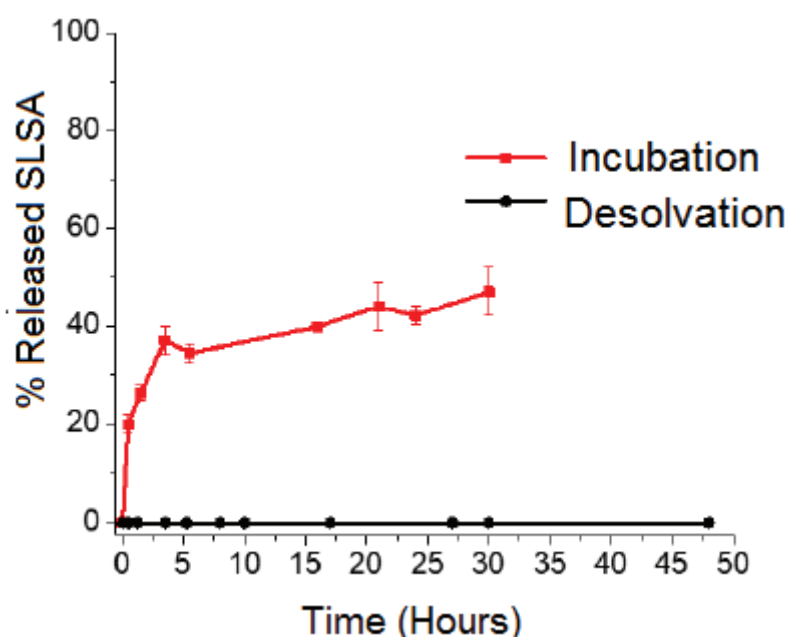
Figure 3.15. Time dependent release dynamics of the SLSA loaded from the cBSA nanoparticles obtained from two different methods: incubation (red) and during nanoparticle preparation step (desolvation method) (black). The amount of drug released was calculated from the dialysis tube by EPR spectroscopy. Dialysis environment was water at 37 ^{0}C.

3.3.3. ATR-FTIR Spectroscopy Study on Difference of SLSA Binding Methods

FTIR spectroscopy was used to examine the molecular structure and conformational changes in cBSA and cBSA NPs were recorded in the absence and

presence of SLSA and their binding with two different loading methods (Figure 3.16). Figure 3.16 shows the FTIR peaks of cBSA, cBSA NPs, SLSA, SLSA loaded cBSA NPs by desolvation method and incubation method. The characteristic peaks of cBSA was observed at 3289 cm^{-1} (amide A, related to N–H stretching), 2948 cm^{-1} (amide B, N–H stretching of NH_3^+ free ion), 1650 cm^{-1} (amide I, C=O stretching), 1531 cm^{-1} (amide II, related to C–N stretching and N–H bending vibrations), 1393 cm^{-1} (CH_2 bending groups), and 1253 cm^{-1} (amide III, related to C–N stretching and N–H bending). The strongest bands are related to proteins secondary structure and its conformation (Source: Kong and Yu, 2007; Rohiwal et al., 2015; Rogers et al., 2014). The spectra of cBSA NPs and SLSA loaded NPs exhibited these characteristic bands of the protein and SLSA structure shifted slightly as shown in figure 3.17. When compared to cBSA with cBSA NPs and SLSA loaded cBSA NPs, a slight shift in the bands was found by the FTIR spectrum observations. The related changes in the amide I, II, and III bands confirm the formation of cBSA NPs and SLSA-loaded NPs.
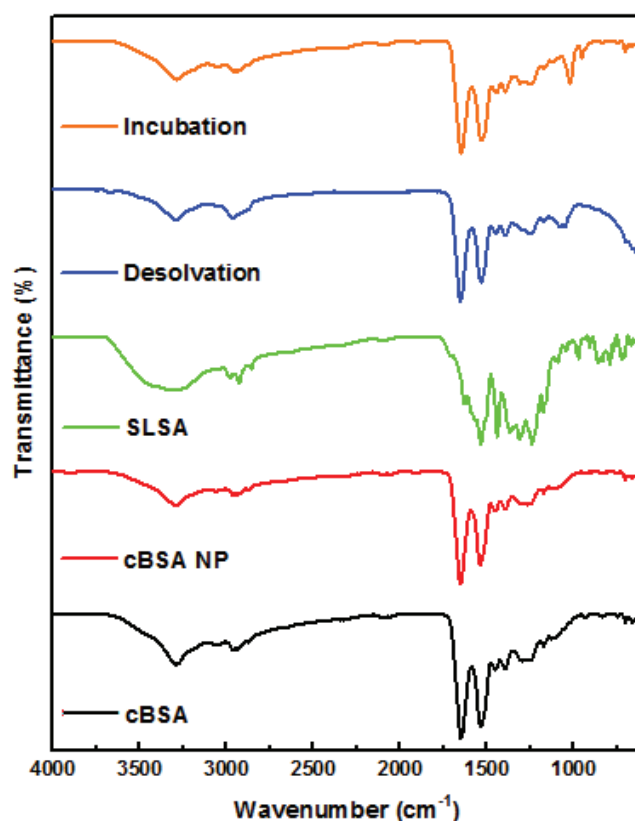
Figure 3.16. FTIR spectra of cBSA (black), cBSA NP (red), SLSA (green), SLSA loaded cBSA NP by desolvation method (blue), and SLSA loaded cBSA NP by incubation method (orange).
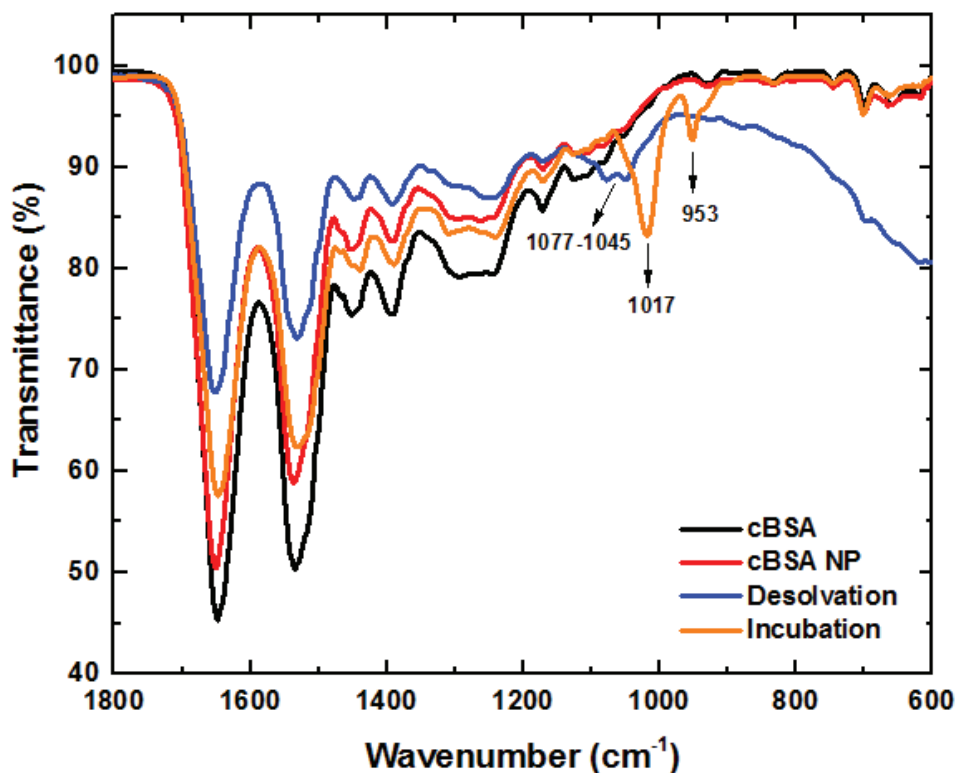
Figure 3.17. FTIR spectra of cBSA (black), cBSA NP (red), SLSA loaded cBSA NP by desolvation method (blue), and SLSA loaded cBSA NP by incubation method (orange) between 1800-600 cm^{-1} wavenumber range.

Peaks of SLSA were observed at 3298 cm^{-1} (O-H stretching), 1625 cm^{-1} (C-C aromatic stretching), 1310 cm^{-1} (C-N stretching from aromatic), 1372 cm^{-1} (N-O symmetric stretching, related to nitroxyl group), 1236 cm^{-1} (C-N stretching), between 1040-1019 cm^{-1} (C-N aliphatic stretching), ~900 cm^{-1} (O-H bending from carboxyl group of SA) and between 800-700 cm^{-1} (N-H wagging) (Figure 3.16 (green)). In the desolvation method, loading of SLSA can be observed by comparing with cBSA in the FTIR spectrum because it mainly affects the protein. In addition to the slightly shifts and intensity decreases in the peaks of the drug loaded nanoparticle, we observed new signals between 1077-1045 cm^{-1} unlike cBSA. Also, we compared the SLSA loaded cBSA NPs prepared by incubation method and cBSA NPs. We found that all main peaks slightly shifted, and intensity of the drug loaded nanoparticles decreased. SLSA signals were observed at 1017 cm^{-1} and 953 cm^{-1}. These signals were originated from C-N aliphatic stretching and O-H bending of carboxyl group of SLSA.

When the desolvation and incubation methods were compared, we can say that the SLSA loaded nanoparticle gives more distinct FTIR signals with the incubation method. The main reason for this is that the drugs attach to the nanoparticle's surfaces in the incubation method and the effect on the structure of the albumin nanoparticle can be observed more easily. In the desolvation method, drugs are first bound to protein and then converted into nanoparticles. SLSA is attached to the inner layers of the nanoparticles rather than their surface and these bindings are difficult to detect as prominent peaks in the FTIR spectrum.

CHAPTER 4

CONCLUSION

In order to increase anionic drug carrying ability of albumin nanoparticles, we produced cationic albumin nanoparticles using desolvation method. The positive surface charge provided a great advantage in the transport of negatively charged drugs. Unlike the literature, BSA protein was first transformed into cationic and then converted into nanoparticles. For this purpose, ethylenediamine was attached to albumin through amino acids with their carboxyl side groups. The zeta potential of the obtained cationic BSA (cBSA) protein was increased from -11 mV to +25 mV. Then, desolvation method was applied to obtain nanoparticles. The sizes of the nanoparticles obtained by using acetonitrile as a solvent in the desolvation method which were found around 200 nm with surface zeta potentials averaging +38 mV.

Salicylic acid is a pain relief which was used as a model drug to demonstrate the efficacy of the cBSA nanoparticles in drug transportation. The salicylic acid loading ability of nanoparticles produced from anionic BSA protein is very low. In this study, cationic nanoparticles were prepared as alternative to anionic BSA nanoparticles in the transportation of salicylic acids.

Firstly, UV-Vis spectroscopy was used to analyze the loading of SA into nanoparticles. Throughout the desolvation process, SA was combined with cBSA in various ratios. SA was loaded in cBSA NPs with a maximum drug loading of 5.6 wt % at SA:cBSA molar ratios (35:1). However, at low SA:BSA ratios, SA was not loaded in native anionic BSA NPs. Despite this, it was loaded at high SA:BSA ratios which was smaller than that of cBSA NPs with a maximum drug loading of 3.0 wt %. This could be explained by decrease in the pH value of SA and BSA mixture at higher SA concentrations. Drug release properties of cBSA NPs and BSA NPs were also different. SA release behavior of cBSA NPs was slower than that of BSA NPs. Furthermore, SEM analyses revealed that drug loading reduced the average size of cBSA NPs from 200 nm to 100 nm while raising the average size of BSA NPs from 100 nm to 275 nm. This is because the pH of the SA-BSA mixture approached the isoelectric point of BSA, favoring BSA-BSA interactions.

In order to monitor the SA by EPR spectroscopy, it was labeled with a stable electron spin radical 4-amino TEMPO. cBSA nanoparticles were prepared with a spin labeled salicylic acid (SLSA): cBSA ratio of 7:1. Drug loaded cBSA nanoparticles were prepared by two different methods; after nanoparticle preparation (incubation), and during nanoparticle preparation (desolvation). As a result of the incubation method, 93% of the drug was remained in the cBSA nanoparticle, while approximately 50% of the drug added during the desolvation method remained in the cBSA nanoparticle. On the other hand, while 15% drug loading was achieved with incubation in drug loading experiments in anionic BSA nanoparticles, it was observed that the only 4% of drug loading was achieved when the drug was added during the nanoparticle preparation step. These showed that cBSA nanoparticles are much better carriers for SLSA. This is because the drug is negatively charged, and the carrier is positively charged. The amount of loaded drug in the nanoparticles was found by EPR spectroscopy. Unlike the studies in which other characterization techniques were used, a more accurate calculation could be made by measuring both the drug loaded in the nanoparticle and the unbound drug by EPR spectroscopy. Again, in the experiments of drug release from the nanoparticle, the detection of the drug remaining in the nanoparticle was made by measuring the nanoparticles by using EPR spectroscopy. The high drug loading efficiency obtained in the incubation experiment appeared as rapid release in the release experiments. However, the drug release was very slow afterwards. This shows that there are two types of attachment. While the drugs on the surface of the nanoparticle are released quickly, the drugs inside are released much more slowly. At the end of 30 hours, still 54% of the drug remains in the nanoparticle. On the other hand, the release of the added drug from the nanoparticle during the desolvation method was not observed even after 48 hours. This shows that the drug was trapped in the nanoparticle is not released. It also supports the results of the binding analysis obtained by FTIR spectroscopy. Conformational changes and binding sides of drug loading on albumin were investigated using by two different methods. It demonstrates that drugs were mostly bound to the surfaces of the nanoparticles in the incubation process, while drugs were mostly bound to the inner layers of the nanoparticles by desolvation method.

In our study, we showed that the cationic serum albumin protein has a high carrying capacity for anionic drugs, and we showed that EPR spectroscopy can also be used in drug transport and release studies beside UV-Vis spectroscopy. Also, we showed

the binding types of drug to the nanoparticle with different loading methods by using FTIR spectroscopy.

REFERENCES

Abbasi, S.; Paul, A.; Shao, W.; Prakash, S. Cationic albumin nanoparticles for enhanced drug delivery to treat breast cancer: preparation and in vitro assessment. *Journal of Drug Delivery*. **2012**, 686108.

Akdogan, Y.; Emrullahoglu, M.; Tatlıdil, D.; Ucuncu, M.; Cakan-Akdogan, G. EPR Studies of Intermolecular Interactions and Competitive Binding of Drugs in a Drug–BSA Binding Model. *Physical Chemistry Chemical Physics.* **2016**, 18, 22531–22539.

Akdogan, Y.; Junk, M. J. N.; Hinderberger, D. Effect of Ionic liquids on the solution structure of human serum albumin. *Biomacromolecules*. **2011**, 12, 1072-1079.

Akdogan, Y.; Hinderberger, D. Solvent-induced protein refolding at low temperatures. The *Journal of Physical Chemistry B*. **2011**, 115, 15422-15429.

Akdogan, Y.; Reichenwallner, J.; Hinderberger, D. Evidence for water-tuned structural differences in proteins: An approach emphasizing variations in local hydrophilicity. *PLOS ONE*. **2012**, 7(9), 45681.

Amann, R.; Peskar, B.A. Anti-inflammatory effects of aspirin and sodium salicylate. *European Journal of Pharmacology*. **2002**, 447(1), 1–9.

An, F.F.; Zhang, X.H. Strategies for Preparing Albumin-based Nanoparticles for Multifunctional Bioimaging and Drug Delivery. *Theranostics*. **2017**, 7(15), 667-3689.

Bamrungsap, S.; Zhao, Z.; Chen, T.; Wang, L.; Li, C.; Fu, T.; Tan, W. Nanotechnology in therapeutics: a focus on nanoparticles as a drug delivery system. *Nanomedicine*. **2012**, 7(8), 1253–1271.

Barenholz, Y. Doxil_d the first FDA-approved nano-drug: lessons learned. *Journal of Control Release.* **2012**, 160, 117-34.

Benvidi, A.; Rezaeinasab, M.; Gharaghani, S.; Abbasi, S.; Zare, H. R., Experimental and theoretical investigation of interaction between bovine serum albumin and the mixture of caffeic acid and salicylic acid as the antioxidants. *Electrochimica Acta*. **2017**, 255, 428-441.

Bhushan, B.; Khanadeev, V.; Khlebtsov, B.; Khlebtsov, N.; Gopinath, P. Impact of albumin based approaches in nanomedicine: Imaging, targeting and drug delivery. *Advances in Colloid and Interface Science.* **2017**.

Bronze-Uhle, E.S., Costa, B.C., Ximenes, V.F., Lisboa-Filho, P.N. Synthetic nanoparticles of bovine serum albumin with entrapped salicylic acid. *Nanotechnology, Science and Applications.* **2017**, 10, 11–21.

Byeon, H.J.; Thao, L.Q.; Lee, S.; Min, S.Y.; Lee, E.S.; Shin, B.S.; Choi, H.G.; Youn, Y.S. Doxorubicin-loaded nanoparticles consisted of cationic- and mannose-modified-albumins for dual-targeting in brain tumors. *Journal of Controlled Release*. **2016**, 225, 301–313.

Chandorkar, Y.; Bhagat, R. K.; Madras, G.; Basu, B., Cross-linked, biodegradable, cytocompatible salicylic acid based polyesters for localized, sustained delivery of salicylic acid: an in vitro study. *Biomacromolecules*. **2014**, 15(3), 863-875.

Das, S., Banerjee, R., Bellare, J. Aspirin loaded albumin nanoparticles by coacervation: implications in drug delivery. *Trends in Biomaterials & Artificial Organs*. **2005**, 18, 203-212.

Dasgupta, Q.; Chatterjee, K.; Madras, G., Controlled release of salicylic acid from biodegradable cross-linked polyesters. *Molecular pharmaceutics*. **2015**, 12 (9), 3479-3489.

Demirkurt, B., Akdogan, Y. Development of an ionic liquid based method for the preparation of albumin nanoparticles. *ChemistrySelect*. **2018**, 3, 9940-9445.

Demirkurt, B., Cakan-Akdogan, G., Akdogan, Y. Preparation of albumin nanoparticles in water-in-ionic liquid microemulsions*, Journal of Molecular Liquids*. **2019**, 295, 111713.

Elzoghby, A.O.; Samy, W.M.; Elgindy, N.A. Albumin-based nanoparticles as potential controlled release drug delivery systems. *Journal of Controlled Release*. **2012**, 157, 168–182.

Fajer, P.G. Site directed spin labeling and pulsed dipolar electron paramagnetic resonance (double electron-electron resonance) of force activation in muscle. *Journal of Physics: Condensed Matter*. **2005**, 17(18), 1459.

Fielding, L.; Rutherford, S.; Fletcher, D., Determination of protein–ligand binding affinity by NMR: observations from serum albumin model systems. *Magnetic resonance in Chemistry*. **2005**, 43(6), 463-470.

Ghuman, J.; Zunszain, P.A.; Petitpas, I.; Bhattacharya, A.A.; Otagiri, M.; Curry, S. Structural basis of the drug-binding specificity of human serum albumin. *Journal of Molecular Biology*. **2005**, 353, 38-52.

Goodman, B.A.; Hall, P.L. Electron paramagnetic resonance spectroscopy. *Clay Mineralogy: Spectroscopic and Chemical Determinative Method. Chapter 5*. **1994**, 173-225.

Gupta, R.A.; Dubois, R.N. Colorectal cancer prevention and treatment by inhibition of cyclooxygenase-2. *Nature Reviews Cancer*. **2001**, 1(1), 11–21.

Han, J.; Wang, Q.; Zhang, Z.; Gong, T.; Sun, X. Cationic bovine serum abumin based self-assembled nanoparticles as siRNA delivery vector for treating lung metastatic cancer, *Small*. **2014**, 10, 524–535.

Hassanin, I.; Elzoghby, A. Albumin-based nanoparticles: a promising strategy to overcome cancer drug resistance. *Cancer Drug Resistance*. **2020**, 3, 930-46.

Hauenschild, T.; Reichenwallner, J.; Enkelmann, V.; Hinderberger, D. Characterizing Active Pharmaceutical Ingredient Binding to Human Serum Albumin by Spin-Labeling and EPR Spectroscopy. *Chemistry-A European Journal*. **2016**, 22(36), 12825-12838.

Hubbell, W.L.; Cafiso, D.S.; Altenbach, C. Identifying conformational changes with sie-directed spin labeling. *Nature structural biology*. **2000**, 7(9), 735-739.

Jeschke, G.; Polyhach, Y. Distance measurements on spin-labelled biomacromolecules by pulsed electron paramagnetic resonance. *Physical Chemistry Chemical Physics*. **2007**, 9(16), 1895-1910.

Karami, K.; Jamshidian, N.; Hajiaghasi, A.; Amirghofran, Z. BSA nanoparticles as controlled release carriers for isophethalaldoxime palladacycle complex; synthesis, characterization, in vitro evaluation, cytotoxicity and release kinetics analysis. *New Journal of Chemistry*. **2020**, 44, 4394–4405.

Karimi, M.; Bahrami, S.; Ravari, S.; Zangabad, P.; Mirshekari, H.; Bozorgomid, M.; Shahreza, S.; Sori, M.; Hamblin, M., Albumin nanostructures as advanced drug delivery systems. *Expert Opinion on Drug Delivery*. **2016**, 13, 1609-1623.

Kattnig, D.R.; Akdogan, Y.; Lieberwirth, I.; Hinderberger, D. Spin probing of supramolecular structures in 1-butyl-3-methyl-imidazolium tetrafluoroborate/water mixtures. *Molecular Physics: An International Journal at the Interface Between Chemistry and Physics*. **2013**, 111(18-19), 2723-2737.

Kennon, S.; Tasch, E.G.; Arm, R.N.; Wig, P.P. The relationship between plaque scores and the development of caries in adult dentition. *Clinical Preventive Dentistry*. **1979**, 1, 26-31.

Khanbabaie, R.; Jahanshahi, M. Revolutionary Impact of Nanodrug Delivery on Neuroscience. *Current Neuropharmacology,* **2012***, 10,* 370-392.

Komiya, K.; Nakamura, T.; Nakashima, C.; Takahashi, K.; Umeguchi, H.; Watanabe, N.; Sato, A.; Takeda, Y.; Kimura, S.; Sueoka-Aragane, N. SPARC is a possible predictive marker for albumin-bound paclitaxel in non-small-cell lung cancer. *OncoTargets Ther*. **2016**, 9, 6663–6668.

Kong, J.; Yu, S. Fourier transform infrared spectroscopic analysis of protein secondary Structures. *Acta Biochimica et Biophysica Sinica.* **2007**, 39, 549–559.

Kudarha, R.R. and Sawant, K.K. Albumin based versatile multifunctional nanocarriers for cancer therapy: Fabrication, surface modification, multimodal therapeutics and imaging approaches. *Materials Science & Engineering C*. **2017**, 81, 607–626.

Langer, K.; Balthasar, S.; Vogel, V.; Dinauer, N.; Briesen, H.V.; Schubert, D. Optimization of the preparation process for human serum albumin (HSA) nanoparticles. *International Journal of Pharmaceutics*. **2003**, 257, 169–180.

Lee, J.N.; Park, C.; Whitesides, G.M. Solvent compatibility of poly (dimethylsiloxane)-based microfluidic devices. *Analytical Chemistry*. **2003**, 75, 6544–6554.

Li, C.; Wang, J.; Wang, Y.; Gao, H.; Wei, G.; Huang, Y.; Yu, H.; Gan, Y.; Wang, Y.; Mei, L.; Chen, H.; Hu, H.; Zhang, Z.; Jin, Y. Recent progress in drug delivery. *Acta Pharmaceutica Sinica B*. **2019**, 9(6), 1145-1162.

Lohcharoenkal, W.; Wang, L.; Chen, Y.C.; Rojanasakul, Y. Protein Nanoparticles as Drug Delivery Carriers for Cancer Therapy. *BioMed Research International*. **2014**, 1-12.

Lopes, C. E., Langoski, G., Klein, T., Ferrari, P. C., Farago, P. V. A simple HPLC method for the determination of halcinonide in lipid nanoparticles: development, validation, encapsulation efficiency, and in vitro drug permeation. *Brazilian Journal of Pharmaceutical Science*. **2017**, 53, 1-9.

Loureiro, A.; Azoia, N.G.; Gomes, A.C.; Cavaco-Paulo, A. Albumin-Based Nanodevices as Drug Carriers. *Current Pharmaceutical Design*. **2016**, 22, 00.

Meng, M., Feng, Y., Guan, W., Liu, Y., Xi, Y., Yan, Y. Selective separation of salicylic acid from aqueous solutions using molecularly imprinted nano-polymer on wollastonite synthesized by oil-in-water microemulsion method. *Journal of Industrial and Engineering Chemistry*. **2014**, 20(6), 3975–3983.

Müller, R.H.; Jacobs, C.; Kayser, O. Nanosuspensions as particulate drug formulations in therapy: rationalefor development and what we ca expect for the future. *Advanced Drug Delivery Reviews.* **2001**, 47(1), 3–19.

Ni, Y.; Su, S.; Kokot, S., Spectrofluorimetric studies on the binding of salicylic acid to bovine serum albumin using warfarin and ibuprofen as site markers with the aid of parallel factor analysis. *Analytica Chimica Acta*. **2006**, 580(2), 206-215.

Nowatzki, P.J., Koepsel, R.R., Stoodley, P., et al. Salicylic acid-releasing polyurethane acrylate polymers as anti-biofilm urological catheter coatings. *Acta Biomaterialia*. **2012**, 8(5), 1869–1880.

Paterson, J.R.; Lawrence, J.R. Salicylic acid: a link between aspirin, diet and the prevention of colorectal cancer. *QJM: International Journal of Medicine*. **2001**, 94(8), 445–448.

Prasanth, S.; RitheshRaj, D.; Vineeshkumar, T.V.; Thomas, R.K.; Sudarsanakumar C. Exploring the interaction of L-cysteine capped CuS nanoparticles with Bovine Serum Albumin (BSA): A Spectroscopic study. *RSC Advances*. **2016**, 1-29.

Rahimnejad, R.; Mokhtarian, N.; Ghasemi, M. Production of protein nanoparticles for food and drug delivery system. *African Journal of Biotechnology*. **2009**, 8(19), 4738-4743.

Ritger, P.L.; Peppas, N.A. A simple equation for description of solute release II. Fickian and anomalous release from swellable devices. *Journal of Controlled Release*. **1987**, 5, 37–42.

Rizk, H.A.; Elanwa, I.M. Dipole moments of glycerol, isopropyl alcohol, and isobutyl alcohol, Can. *Journal of Chemistry*. **1968**, 46, 507–513.

Rogers, M.A.; Yan, Y.F.; Ben-Elazar, K.; et al. Salicylic acid (SA) bioaccessibility from SA-based poly (anhydride-ester). *Biomacromolecules*. **2014**, 15(9), 3406–3411.

Rohiwal, S.S.; Satvekar, R.K.; Tiwari, A.P.; Raut, A.V.; Kumbhar, S.G; Pawar, S.H. Investigating the influence of effective parameters on molecular characteristics of bovine serum albumin nanoparticles. *Applied Surface Science*. **2015**, 334, 157–164.

Saha, A.; Pradhan, N.; Chatterjee, S.; Singh, R.K.; Trivedi, V.; Bhattacharyya, A.; Manna, D. Fatty-amine-conjugated cationic bovine serum albumin nanoparticles for target-specific hydrophobic drug delivery. *ACS Applied Nano Materials*. **2019**, 2, 3671–3683.

Sahu, I.D.; Lorigan, G.A. Electron Paramagnetic Resonance as a Tool for Studying Membrane Proteins. *Biomolecules*. **2020**, 10, 763.

Savjani, K.T.; Gajjar, A.K.; Savjani, J.K. Drug Solubility: Importance and Enhancement Techniques. *ISRN Pharmaceutics*. **2012**, 10.

Sozer, S.C.; Egesoy, T.O.; Basol, M.; Cakan-Akdogan, G.; Akdogan, Y. A simple desolvation method for production of cationic albumin nanoparticles with improved drug loading and cell uptake. *Journal of Drug Delivery Science and Technology*. **2020**, 60, 101931.

Spasojević, I. Free radicals and antioxidants at a glance using EPR spectroscopy. *Critical Reviews in Clinical Laboratory Sciences*. **2011**, 48(3), 114-142.

Steinhoff H.J. Inter-and intra-molecular distances determined by EPR spectroscopy and site-directed spin labeling reveal protein-protein and protein-oligonucleotide interaction. *Walter de Gruyter*. **2004**, 385(10), 913-920.

Storp, B.V.; Engel, A.; Boeker, A.; Ploeger, M.; Langer, K. Albumin nanoparticles with predictable size by desolvation procedure, *Journal of Microencapsulation*. **2012**, 29, 138–146.

Sun, T.; Zhang, Y.S.; Pang, B.; Hyun, D.C.; Yang, M.; Xia, Y. Engineered Nanoparticles for Drug Delivery in Cancer Therapy. *Angewandte Chemie International Edition*. **2014**, 53, 12320 – 12364.

Tang, S.Z., June, S.M., Howell, B.A., Chai, M. Synthesis of salicylate dendritic prodrugs. *Tetrahedron Letters*. **2006**, 47(44), 7671–7675.

Tatlidil, D. Study of Drug Transportation by ESR Spectroscopy. Msc Thesis, İzmir Institute of Technology, **2018**.

Tatlidil, D.; Ucuncu, M.; Akdogan, Y.; Physiological Concentrations of Albumin Favor Drug Binding. *Physical Chemistry Chemical Physics*. **2015**, 17, 22678-22685.

Tiwari, G.; Tiwari, R.; Sriwastawa, B.; Bhatiz, L.; Pandey, S.; Bannerjee, S.K. Drug delivery systems: An updated review. *International Journal of Pharmaceutical Investigation*. **2012**, 2, 2-11.

Verma, A.; Stellacci, F. Effect of surface properties on nanoparticle- cell interactions. *Small.* **2010**, 6, 12–21.

Whitaker-Brothers, K., Uhrich, K. Investigation into the erosion mechanism of salicylate-based poly(anhydride-esters). *Journal of Biomedical Materials Research Part A*. **2006**, 76(3), 470–479.